Radiolabeled acetate PET in oncology imaging -Studies on head and neck cancer, prostate cancer and normal distribution

Aijun Sun

Department of Radiation Sciences, Oncology
Umeå University
SE-90187 Umeå
Sweden 2010

Department of Radiation Sciences, Oncology
Umeå University
SE-90187 Umeå
Sweden

Copyright © Aijun Sun
ISBN 978-91-7264-967-5
ISSN 0346-6612
Printed by Print&Media, Umeå University
March 2010

To my husband, daughter and parents

Contents

Contents **5**

1 Abstract **6**

2 List of papers **7**

3 Abbreviations **8**

4 Introduction **9**

4.1 General background of head and neck cancer and prostate cancer 9

4.2 RT and tumor bioenergy metabolism 10

4.3 PET Principle 12

4.4 FDG PET 13

4.5 C-AC PET 14

4.6 F-AC PET 19

5 Aims of the study **21**

6 Materials and methods **22**

6.1 Patients and animals 22

6.2 PET imaging protocols 24

6.3 PET imaging analysis 25

6.4 Statistics 29

7 Results and discussion **30**

7.1 Detecting primary tumors and lymph node metastases 30

7.2 Delineating tumor volumes 34

7.3 Tumor oxidative metabolism during RT 36

7.4 Tumor perfusion during RT 39

7.5 Correlation of tumor oxidative metabolism, perfusion and glycolysis 41

7.6 Tumor C-AC SUV during RT 42

7.7 SUV, CT HU of benign and malignant lymph node in prostate cancer 43

7.8 Kinetics of C-AC in benign lymph nodes and recurrent prostate cancer 44

7.9 Normal distribution of C-AC and F-AC in animals 47

8 Conclusions **53**

9 Acknowledgements **54**

10 References **56**

1 Abstract

The use of positron emission tomography (PET) for imaging in oncology has grown rapidly in recent years. 2-[^{18}F]-fluorodeoxyglucose (FDG) is the most common tracer of PET, although drawbacks exist. Radiolabeled 1-[^{11}C]-acetate (C-AC) is a simple probe for evaluation of perfusion, anabolism (lipogenesis) and catabolism (oxidative metabolism) in all living tissues. This study explored the potential of AC PET in head and neck cancer, benign and malignant lymph nodes in prostate cancer and normal distribution.

In head and neck cancer, C-AC PET detected more primaries and lymph node metastases than FDG PET. The mean primary tumor volumes delineated by C-AC was 51% larger than that of FDG before radiotherapy (RT). Both FDG and C-AC PET tumor volumes must be carefully validated before used in clinical routine. Baseline tumor clearance rate ($k_{mono)}$ was higher in complete responders (CR) than that in partial responders (PR). k_{mono} tended to correlate inversely with FDG SUV at baseline. Radiosensitive tumors might rely predominantly on oxidative metabolism for their biogenetic needs. k_{mono} increased in PR during RT. The potential reversibility of impaired k_{mono} in radioresistant tumors imply that treatment targeting the intermediary metabolism might improve the outcome. Tumor relative perfusion index (rF) and k_{mono} were coupled in CR throughout the RT, but not in PR. Dynamic C-AC PET provides a new non-invasive method to simultaneously evaluate the tumor oxidative metabolism and perfusion which link the RT response in patients by a single tracer injection.

In prostate cancer, elevated C-AC accumulation is common in benign inguinal lymph nodes, probably due to increased lipogenesis rather than lymphatic drainage. CT Hounsfield unit of benign nodes was lower than that of metastases, suggesting that density measurement using CT might improve the specificity of nodal staging of prostate cancer.

A novel tracer 2-[^{18}F]-fluoroacetate (F-AC) was synthesized and used for dynamic PET-CT imaging in animals. Compared with C-AC PET-CT, F-AC showed prolonged blood retention, no detectable trapping in myocardium and salivary glands, rapid excretion from liver to bile and urine and de-fluorination resulting in intensive skeletal activity. F-AC does not mimic the normal physiologic path of C-AC and appears to be of little use for assessment of perfusion, intermediary metabolism or lipogenesis.

Key words: ^{11}C-acetate, ^{18}F-fluoroacetate, PET, Head and neck cancer, Staging, Delineating tumor volume, Clearance rate, Perfusion, RT, Treatment outcome, Benign and malignant lymph node, Prostate cancer, Normal distribution.

2 List of papers

This thesis is based on the following papers, which will be referred to in the text by their roman numerals:

I. **Aijun Sun**, Jens Sörensen, Mikael Karlsson, Ingela Turesson, Bengt Langström, Per Nilsson, Lena Cederblad, Jan Bertling, Katrine Riklund, Silvia Johansson. 1-[^{11}C]-acetate PET imaging in head and neck cancer - a comparison with ^{18}F-FDG PET: implication for staging and radiotherapy planning. *Eur J Nucl Med Mol Imaging*, 2007 34(5): 651-657.

II. **Aijun Sun**, Silvia Johansson, Ingela Turesson, Alexandru Dasu, Jens Sörensen. Imaging tumor perfusion and oxidative metabolism in patients with head and neck cancer using 1-[^{11}C]-acetate PET during radiotherapy - preliminary results. *Submitted*, 2010.

III. **Aijun.sun,** Cecilia Wassberg, Silvia Johansson, Ingela Turesson, Jens Sörensen. Characterizing benign and malignant lymph nodes using 1-[^{11}C]-acetate PET-CT in biochemical relapsing prostate cancer patients. *Submitted* 2010.

IV. Örjan Lindhe, **Aijun Sun**, Johan Ulin, Obaidur Rahman, Bengt Långström, and Jens Sörensen. [^{18}F]-fluoroacetate is not a functional analogue of [^{11}C]-acetate in normal physiology. *Eur J Nucl Med Mol Imaging*, 2009 36(4): 1453-1459.

Paper Ⅰ and Paper Ⅳ were reprinted with permission from the publishers.

3 Abbrevations

SCC	Squamous cell carcinoma
CT	X-ray computed tomography
MRI	Magnetic resonance imaging
PSA	Prostate specific antigen
RT	Radiotherapy
ATP	Adenosine triphosphate
FDG	2-deoxy-2-[^{18}F]-fluoro-D-glucose
PET	Positron emission tomography
C-AC	1-[^{11}C]-acetate
F-AC	2-[^{18}F]-fluoroacetate
HCC	Hepatocellular carcinoma
k_{mono}	Clearance rate
FAS	Fatty acid synthase
MCT	Mono-carboxylate transporter
ACS	Acetyl-CoA synthetase
SUV	Standardized uptake value
TAC	Time activity curve
ROI	Region of interest
rF	Relative perfusion index
CR	Completed response
PR	Partial response
ANOVA	Analysis of variance
Tglu	Tumor glucose uptake
HU	Hounsfield unit
M-LN	lymph node metastases
B-LN	Benign superfacial lymph nodes
L/S	Ratio of long to short axis

4 Introduction

4.1 General background of head and neck cancer and prostate cancer

Cancer is one of the most life-threatening diseases with the characteristics of uncontrolled growth, invasion to surrounding tissue and distant metastasis. Statistic data from World Cancer Report showed that 12.4 million patients were newly diagnosed and 7.6 million patients died from various cancers in approximate 6.7 billion people of world wide population in year 2008 [1].

4.1.1 Head and neck cancer

More than 40,000 new cases are diagnosed head and neck cancer each year in the USA, accounting for 2-3% of all cancers [2, 3]. The incidence rate has been increasing. Male to female ratio is greater than 2:1. Life style and local environmental factors, such as smoking, alcoholism, virus (Epstein-Barr and papilloma virus) infection have etiological roles in head and neck cancer. More than 90% head and neck cancers are squamous cell carcinoma (SCC). According to the degree of hornification, head and neck SCC is graded into three groups, well (>75%), moderate (25-75%) and poorly (<25%) cell differentiated. SCC can grow superficially as well as invade into deep soft tissue, adjacent mucosa, muscular, cartilaginous and bone structure. The TNM staging system determines treatment strategy and predicts prognosis. Patients with head and neck cancer are curable when diagnosed at an early stage [4]. Therefore, it is crucial to precisely define TNM stage before treatment of the individual patient.

Conventional imaging modalities such as computed tomography (CT), magnetic resonance imaging (MRI) and ultrasonography are the most often used tools for imaging in oncology. These techniques provide excellent anatomic information of tumor, are used for tumor TNM staging and monitoring tumor response to treatment. Still, all these techniques have inherent limitations and provide only little information about the biological activity of the tumor.

4.1.2 Prostate cancer

Prostate cancer is the most common malignancy of males in developed countries and the second leading cause of death next to lung cancer in the USA [5]. In 2008, 186,000 new cases and 28,600 deaths were registered in the USA. The risk factors of prostate cancer are related to age, race, heredity, diet, life style and other environmental factors. The incidence rate increases gradually over age 50 with a huge difference between races. It is almost ten times higher in North American than in Asian, and this rate is even higher in Afro-American [6].

More than 95% of prostate cancers are adenocarcinomas. Tumor is graded into 2-10 Gleason score, according to the characteristics of cells under microscopy. Higher scores mean more aggressiveness. Primary diagnosis is based on biopsy, CT, MRI and biomarkers such as prostate specific antigen (PSA). Prostate cancer is considered to be slow growing with a relatively good prognosis. However, advanced cancer often invades into the neurovascular, peripheral prostate, seminal vesicles; or spreads to lymph nodes and bones. The five years survival rate for all prostate cancer patients is only 57% in Europe in early nineties [7].

Approximately 30% of prostate cancer patients undergoing treatment will eventually relapse biochemically and have a high risk of developing locally progressive disease and metastasis [8]. PSA is one of the main references for patient follow-up post treatment. In many departments, post operative radiotherapy (RT) is given locally in a relatively blinded fashion when local recurrence is suspected with PSA rise. Malignant loco-regional nodes, if known, should be included in the dose plan with a boost. There are many patients who have rising PSA with undetectable lesions by current imaging modalities. Especially in patients with relatively low PSA relapse. This undetectable lesion is problematic to the radio-oncologist when determining the irradiated area. Therefore, characterizinging benign and malignant lymph node and local recurrence is important for RT treatment planning, thereby increasing the accuracy of the treatment.

4.2 RT and tumor bioenergy metabolism

RT is one of the main treatment options in cancers with the aim to sterilize tumor cells without damage to the surrounding normal tissues. In head and neck cancer, RT has the opportunity to preserve the normal organ function and

provides more cosmetically results compared to surgery. In locally advanced disease, the cure rate of head and neck cancer is poor [9]. The 5-year survival rate is less than 30% when RT is used alone, and 80% of recurrences appear within 2 years [10]. Treatment failure is correlated with many factors such as staging, tumor volume delineation for RT dose planning, tumor biologic characteristics, and the microenvironment. Among them, oxygenation is one of the most important factors correlating with radiosensitivity and treatment outcome. Poor oxygenation correlates to radioresistance and poor outcome [11]. Intracellullar oxygen is important not only for improving tumor cell DNA damage by RT but is also necessary for the tumor to maintain oxidative metabolism [11, 12]. Tumor hypoxia resulting from insufficient perfusion would force the tumor cell from the mitochondrial respiration towards anaerobic glycolysis for survival. But it is well known that tumor cells share a common glycolysis phenotype even in presence of oxygen [13]. This phenomenon is called the Warburg effect. The tumor is forced from the high production of bioenergy 30 adenosine triphosphates (ATPs) by the completed oxidation of glucose to the rather inferior route of only 2ATPs by glycolysis, and produces a toxic acidic microenviroment due to lactate formation [14, 15]. Warburg attributed this phenomenon to a deranged mitochondrial function, causing impaired oxidative metabolism and promoting cancer survival and progress. A recent study has shown that this bioenergy switch and toxic microenviroment result in facilitated survival of tumor by evading the apoptosis, ultimately leading to local membrane invasion and metastatic spread [16].

The detection of increased tumor glycolysis is well established by 2-fluorodeoxyglucose (FDG) positron emission tomography (PET) in various tumors [17]. However, since Warberg's age, it has been blindly understood that all cancer types depend mainly or only on glycolysis for ATP supply without experimental evidences. In fact, tumor cells rely both on glycolysis and mitochondrial oxidative metabolism for their bioenergetic requirements [13]. In in vitro and animal studies, different tumor cell types differently dominant bioenergetic metabolic pathways [12, 18]. Treatment that only inhibits glycolysis can not effectively kill cancer cells in which there is a preference for using the oxidative metabolism for ATP supply [19]. Deficient oxidative metabolism

correlates with a more malignant phenotype [20] and oxidative metabolism may be a key factor in controlling tumor growth [21]. Studies of the various metabolic pathways in cancer might create new insights into the relation of tumor bioenergetics towards treatment outcome.

4.3 PET principle

PET is an advanced molecular imaging technique. It enables a non-invasive tracing of the physiologic and pathologic processes of the disease qualitatively and quantitatively by measuring radioactivity concentration and/or the reaction rates of the tracer throughout the body. The positron emitting radionuclides ^{11}C, ^{15}O, ^{13}N and ^{18}F used for labeling compounds or tracers for PET are produced by cyclotrons and have short half lives from 2-110 minutes. After the radionuclide labeled molecular compound is injected into the body, the unstable radionuclide decays by emitting a positron particle that collides with a nearby electron and both are annihilated, releasing two oppositely directed 511kev γ photons. The photons strike the detectors which surround the studied object in the field of view. The coincidence events are recorded by the detector and stored in the workstation. Subsequently, the collected data are reconstructed and stored in datasets that are converted into three dimensional images with variable color scales, representing the actual radioactivity concentration within the body (Figure 1).

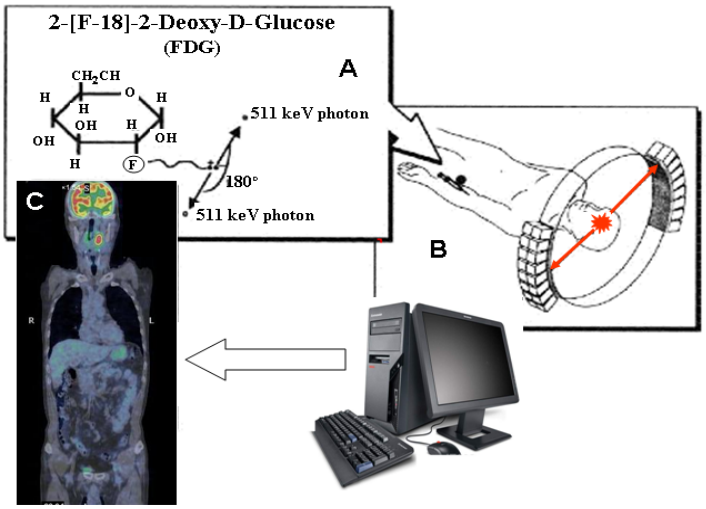

Figure 1 The principle of PET. Positron emitted ^{18}F- FDG was produced by cyclotron，annihilation occurred after injection (A). Dual 511kev γ photons strike the detectors simultaneously and were recorded (B). Collected data was converted to images (C). Adopted From Phelps ME. (J Nucl Med 2000, 41: 661-681)

4.4 FDG PET

FDG is the most common tracer of PET in oncology imaging. It is an analog of glucose with 18-Fluorine substituting an hydroxyl group in the second position of the glucose molecule. As a result of this substitution, FDG only participate in the initial enzymatic reactions of glucose metabolism. After FDG is injected intravenously, it competes with normal glucose and is transported from plasma to tissue by specific glucose transporters in cell membranes and phosphorylated to ^{18}F-FDG-6-phosphate by the enzyme hexokinase, after which it is trapped in the cells without further metabolism. High uptake of FDG is therefore due to the over-expression of glucose transporters and hexokinase in the tumor cells [22] and only indirectly associated with increased glycolysis. FDG PET has achieved a central role for evaluation of patients with various tumor types. It has been used not only for staging, restaging, distinguishing recurrence, but also for delineating biological target volumes for RT treatment planning; and monitoring tumor response [23-26].

The greatest advantage of FDG PET in head and neck cancer is identifying the recurrent tumor due to the distorted surrounding tissues after treatment in conventional imaging. FDG PET significantly improved the sensitivity (86-100%) and specificity (84-93%) in detecting the recurrence [27-30]. In detection of the primary head and neck cancer, FDG PET is comparable to CT and MRI [31], but significantly superior to CT and MRI in detection of lymph node metastasis [32-36].

There is a growing tendency to take into account the biologic tumor volume in RT planning. The biologic tumor volumes derived from PET has dramatically impacted treatment planning of RT in recent years [37, 38]. Nestle et al [39] reported that tumor volumes changed by 35% when using FDG PET in lung cancer. Wang et al [40] revealed that gross tumor volumes derived from FDG PET were different in 89%(16/18) head and neck cancers compared with CT. Combined anatomic and functional imaging for definition of tumor target has led to improvement in RT. Recent FDG PET studies have focused more on the potential of monitoring tumor response [41], since metabolic changes occur earlier than the morphologic changes. Decreased FDG uptake during or after

therapy has correlated with the tumor remission [17, 42-44]. In tumor non-responder, FDG-PET may provide early evidence to adjust the alternative treatment options timely for individual patient.

However, it is well known that FDG is not a specific tumor marker. Increased uptake may also be found in inflammatory processes, normal organs (salivary gland, tonsil, muscle, floor of the mouth and vocal cord etc), healing tissues, and benign lesions. Although dual time scan may improve the determination of malignant lesions from inflammatory tissues and benign lesions, it is not always efficient [45]. Further, faint or minimal FDG uptake in well differentiated and mucus producing cancers, such as lung bronchioloalveolar carcinoma, prostate cancer, gastrointestinal cancer, hepatocellular carcinoma (HCC), and head and neck cancer, limits the clinical usefulness of FDG PET [46-48].

Despite the limitations of FDG PET, there is no other single tracer can represent the entire tumor biologic profile. Therefore, developing new tracers in PET oncology imaging might help better understand tumor biologic characteristics, eventually improving staging, delineating and monitoring response of tumor towards treatment outcome. Several such tracers are under investigation [49-54].

4.5. 1-[^{11}C]-acetate (C-AC) PET

4.5.1 Application of C-AC PET in research and clinic

Acetate is a physiologic metabolite normally present in the blood at 0.2-0.3mM concentration [55], and has a pivotal role in the intermediary metabolism of all living tissues. In human studies, variable uptake of C-AC has been found in different organs. Pancreas, salivary gland , tonsil , bowel , spleen, heart, bone marrow and sometimes muscle all may have intensive C-AC accumulation. Low retention is normally seen in brain and lung. Intermediate uptake levels are seen in liver and normal prostate. Urinary excretion is minimal.

Radiolabeled C-AC was initially used in coronary disease for measurements of perfusion and oxidative metabolism almost 3 decades ago [56]. It has been proposed that C-AC traces the activity of Krebs cycle in the myocardium. The monoexponential clearance rate of C-AC (k_{mono}) reflects the rate of myocardium

oxidative metabolism. This finding later has been confirmed by the other authors [57] and also studied in the kidneys [58] and astrocytes of brain [59]. The clearance of C-AC results in diminishing radiosignal in PET is contributed to the formation of $^{11}C\text{-}CO_2$, which is a terminal product of oxidative metabolism of C-AC through the Krebs cycle. The $^{11}C\text{-}CO_2$ leaves the tissue, enters the blood stream and is finally exhaled from the lungs.

In recent years C-AC began to be used for PET imaging in various tumors, especially in slow-growing or well differenticated tumors which are not FDG avid. The results have been promising for detecting HCC, lung adenocarcinoma, thymoma and prostate cancer [46, 47, 60, 61]. Shreve et al [62] first reported on C-AC PET in renal disease, they found that C-AC uptake in renal neoplasm reached a peak value in the first several minutes after injection, then followed by a slower clearance in tumor than that in normal parenchyma. Ho et al [46] has found that sensitivity and specificity of C-AC PET in HCC are much higher than that of FDG PET. Interestingly, variable uptake in different tumor components was also observed by dual-tracer studies. Histopathologic corrrelation suggested that C-AC was extracted primarily in well differentiated HCC, while FDG uptake was higher in poorly differentiated HCC. Similar findings were shown by Hwang et al [63] in HCC and Shibata et al [61] in lung adenocarcinoma. Liu et al [64] examined 513 patients with various malignant tumors using C-AC PET. High sensitivity was reported in meningioma (97%), glioma (91%), nasopharyngeal cancer (93%), lymphoma (85%), non small cell carcinoma (81%) and ovarian cancer (76%). Unfortunately, the findings based on this large materials were only described in abstract form.

Lately, the most common use of C-AC PET in oncologic imaging is in prostate cancer [47, 65]. C-AC is more suitable for visualizing prostate cancer, due to the lack of urinary excretion and a favorable tumor-to-background ratio. Most studies have been performed in patients with rising PSA levels after primary treatment with curative intent. There is a clinical need for a imaging modality to locate the recurrent tumor in order to guide the RT planning and further treatment management. Especially so for small lymph node metastases or small regional recurrences at low PSA levels. C-AC PET is more sensitive than FDG PET for

detecting primary and recurrent prostate cancer and regional lymph node metastases [47, 66-69]. Increased C-AC retention in malignant tissue of prostate seems correlated with the upregulation of fatty acid synthase (FAS) expression, which is the key enzyme of lipogenesis [70, 71].

To the best of our knowledge, there is no data of C-AC PET in characterizing benign and metastatic lymph node of prostate cancer. In clinical practice, we have found that high uptake of C-AC was frequently seen in the superficial inguinal node where the lymph node metastasis rarely disseminate [72-75]. These high uptake nodes usually accompany fatty infiltration, as seen on CT and therefore routinely regarded as benign. However, the mechanism of the high uptake in benign node is not fullly understood. It could be caused by cellular anabolic processes similar to those of cancers, or result from radioactive metabolites in lymphatic drainage from the lower extremities. On the other hand， such lymph nodes, if located in the pelvic pathway of lymph node metastasis of prostate cancer, would highly mimic the malignant metastasis. Therefore, characterizing the image based criteria of benign and malignant lymph node might improve the nodal staging .

Different cancer avidity of C-AC and FDG in certain tumors has been found in HCC and lung cancer. Rare data of C-AC PET has been reported in delineating gross tumor volume and monitoring tumor response. Seppala et al [76] using C-AC PET for delineating biologic tumor volume in introprostatic lesion of prostate cancer for dose escalation. C-AC based biologic target volume can theoretically deliver an ultra high dose to tumor without increasing the treatment toxicity. In our own on-going clinical research work, successful hormonal therapy invariably reduced tumor C-AC uptake. These preliminary findings might provide a new method for monitoring the tumor response of biochemical recurrent prostate cancer and metastasis after systemetic treatment, and further to confirm the malignant node when conventional imaging and biopsy can not be accessed. More studies are needed to validate the feasibility of C-AC PET in monitoring the metabolic changes after therapy.

4.5.2 Uptake mechanisms and metabolic pathway of C-AC

The uptake mechanisms and further metabolic pathways of acetate are still not

fully understood. Most of the current knowledge comes from studies utilizing radiolabeled acetates. After C-AC is injected intravenously, it is rapidly cleared from the blood stream and enters the cells by monocarboxylate transporters (MCT) or diffusion. The extraction rate of C-AC is approximately 70% in individual organs and in whole body level [77]. The high extraction rate makes C-AC a 'biochemical microsphere' for PET, and early phase imaging reflects the propotion of perfusion and probably the overall metabolism requirement [78]. In the cells, C-AC is activated and trapped as ^{11}C- acetyl-CoA by Acetyl-CoA synthetase (ACS). There are two distinctive forms of ACS. ACS1 is mainly located in the cytosol and overexpressed in tissues with high active lipogenesis, such as liver, salivery gland, spleen and also many cancers [79]. ACS1 knockdown led to reduced ^{14}C-acetate uptake in tumor cells under nomoxia and hypoxia [80]. ACS2 is expressed in mitochondria, most abundantly in heart and kidney. In the mitochondria, ^{11}C-acetyl-CoA enters the Krebs cycle, either terminally oxidized to ^{11}C-CO_2 in proportion to the rate of oxidative metabolism or used for anabolic processes for lipid and amino acid synthesis and other intermediate metabolism (Figure 2). Yoshimoto et al [54] investigated different tumor cell lines with ^{14}C-acetate, and shown that high tumor uptake of C-AC is attributed mainly to the increased lipogenesis which is needed to build up cell membrane for proliferation. Many enzymes are involved in the lipogenesis, such as ACS, ATP citrate lyase, Acetyl-CoA carboxylase and FAS.

A recent study [81] has shown that ACS1 was expressed only in HCC cell lines with high FDG uptake but low C-AC uptake. While, both ACS1 and ACS2 were highly expressed in HCC cell lines with low FDG uptake and high C-AC uptake. Furthermore, a FAS inhibitor decreased ^{14}C-acetate uptake in prostate cancer. However, even higher dose of FAS inhibitors could not completely inhibit the C-AC uptake [71]. All these findings indicate that there are other mechanisms involved in C-AC uptake of tumor besides the anabolic lipogenesis. So far, most C-AC PET in oncology imaging are concerned with studying the tumor anabolism merely by static measurements of the standardized uptake value (SUV), but not reporting on the potential use of C-AC in studies of oxidative metabolism.

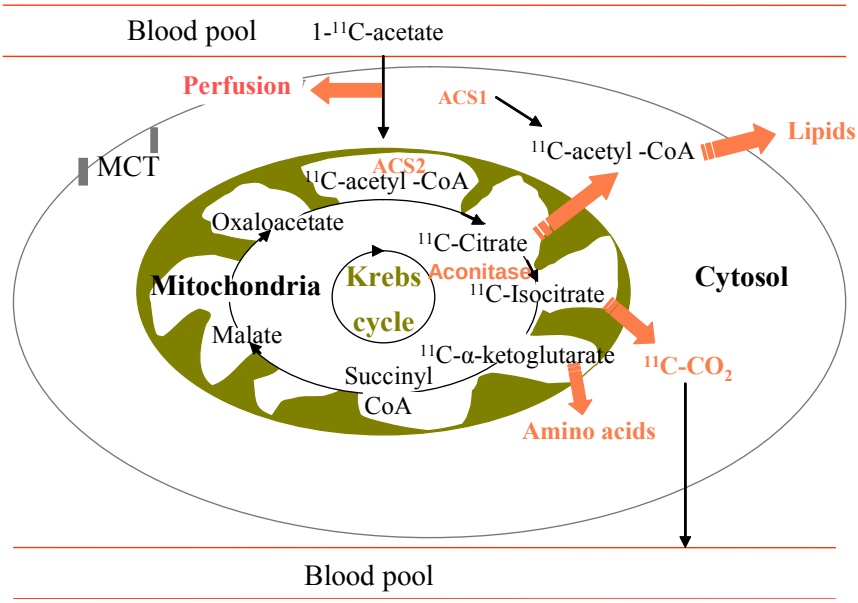

Figure 2 The Metabolic pathway of C-AC Kinetics. MCT = monocarboxylate transportor. ACS = Acetyl-CoA synthetase.

Evidence linking the oxidative metabolism with tumor progress has been growing. Switching tumor cells from glycolysis into mitochondria oxidative metabolism efficiently inhibits cancer growth, indicating that low tumor invasiveness might be functionally linked with maintained oxidative phosphorylation [12]. Oxidative metabolism may be a key factor influencing the tumor growth [21]. However, all these findings are based on in vitro studies. Clearance rate of C-AC in the Krebs cycle as an index of oxidative metabolism in human has been well characterized in myocardium. Meanwhile, only little data involves the oxidative metabolism of C-AC in tumors in vivo, which is oxidized as $^{11}C\text{-}CO_2$ in mitochondria. The lower tumor clearance rate of C-AC compared to normal tissues has been indicated by Yeh et al [82] in the nasopharyngeal carcinoma and Shreve et al [62] in renal cell carcinoma. They proposed that the reduced clearance rate of tumor was caused by the impaired oxidative metabolism and enhanced lipogenesis. Kinetics of C-AC PET may provide an unique tools for investigating tumor biologic characteristics of oxidative metabolism, anabolism of lipogenesis as well as tumor perfusion in vivo.

4.5.3 Tumor perfusion

Perfusion carries oxygen and nutrition to tumor cell and tightly links to patient treatment outcome. Adequate tumor perfusion is not only the prerequisite for tumor oxidative metabolism but also is necessary for successful chemoradiotherapy [12]. High tumor perfusion during the early RT predict low recurrence in cervix cancer. Imaging tumor perfusion during the treatment course may help optimize the treatment strategy. The high extraction rate of kinetic C-AC PET in the early phase has been widely used for evaluating the perfusion of myocardium for two decades. The simplest method for the absolute quantification of the perfusion might be assume zero recirculation of the tracer during the first pass of bolus injection. Yet, it is less practical because the artery input function is still needed. An alternative solution is to derive the artery input function from a substantial main blood vessel or compartment in PET imaging. However in certain region, such as head and neck, the artery input function might be inaccurate due to partial volume effects. Hence, developing a new method to measure the tumor perfusion in this region is warranted.

4.6 2-[^{18}F]-fluoroacetate (F-AC) PET

Numerous kinetic studies of C-AC PET have been performed to measure the perfusion (early phase), oxidative metabolism (rapid clearance reflects oxidation in Krebs cycle) and retention of radioactivity in lipid formation in tumor [61, 62, 83], mostly in well differentiated and slow growing tumor, in which FDG uptake is weak. However, their widespread use is restricted by the logistic problems posed by the short ^{11}C half life of 20 min. Even with a high-yield synthesis at an in-site cyclotron, only limited patients can be performed from a single batch preparation. Furthermore, using ^{11}C labeled endogenous compounds has to analyze the kinetics of tracer biochemical pathways and metabolite correction, more complex than the simple evaluation of accumulation in the static images as FDG in clinics. Based on the other successful fluorination of endogenous compounds in clinical PET imaging, such as choline, tyrosine, thymidine [51, 84, 85], developing long half life of 18-Fluorine labeled acetate is relevant.

Fluoroacetate carries a well known toxicity at high doses [86]. This would not happen at low doses injection in PET imaging. The mechanism of toxicity is partly caused by the formation of fluorocitrate which binds to aconitase and

irreversibly blocks the Krebs cycle. Aconitase is a key enzyme converting citrate to isocitrate (Figure 2). F-AC has been reported as a surrogate marker of C-AC and appears of potential use in prostate cancer and glioblastoma [52, 87, 88]. This might imply that F-AC is a substrate of MCT and ACS enzyme. If the metabolic pathway of F-AC mimics that of C-AC, it might be a useful tracer of PET for measuring perfusion, imaging myocardium oxidative metabolism and evaluating the anabolism of lipogenesis in tissues and cancers. Defluorination of F-AC has been found species dependent and occurred in rodents, with high accumulation of free ^{18}F in bone. Only few data is available on F-AC in normal physiology of advanced mammals, such as baboon.

Based on the information above, we explored C-AC PET in head and neck cancer for staging, delineating tumor volume before RT, imaging tumor oxidative metabolism and perfusion during RT, and characterizing the benign and malignant lymph node metastais of prostate cancer from different aspect of C-AC kinetics. And evaluating the kinetic patterns and normal distribution of novel tracer F-AC in animals and compared to C-AC.

5 Aims of the study

1. To evaluate the feasibility of C-AC PET in detecting and delineating the gross tumor volume for RT planning in head and neck cancer and compare the results with FDG PET.
2. To image tumor oxidative metabolism, perfusion in patients with head and neck cancer using dynamic C-AC PET during RT.
3. To characterize the benign and malignant lymph nodes of biochemically recurrent prostate cancer using C-AC PET.
4. To evaluate the potential of a novel tracer F-AC for imaging perfusion and intermediate metabolism and lipogenesis in animals under normal physiology and compare to C-AC PET.

6 Materials and Methods

6.1 Patients and animals

6.1.1 Head and neck cancer patients (Paper Ⅰ-Ⅱ)

Ten patients with histologically confirmed SCC of the head and neck were studied at baseline (Paper Ⅰ). No patients were treated before the enrollment and all were candidates for RT. Histopathological confirmation was obtained by guided biopsy in all the primary tumors and most lymph node metastases. Five lymph node metastases were diagnosed to be malignant based on the combination of all available information, including 3 months follow up. Conventional staging of the tumors included clinical examination, CT (n = 9) or MRI (n = 1). The clinical characteristics of patients are presented in Table 1. Nine of ten patients were included in Paper Ⅱ.

Table 1 Clinical characteristics of patients.

Patient	Sex	Age(year)	Stage	Location	Histology diff
1	M	77	T4N2cM0	Larynx	Low
2	F	57	T2N0M0	Nose	Moderate
3	M	59	T2N0M0	Nose	High
4	M	53	T3N0M0	Nose/sinus	Low
5	F	67	T4N3M1	Tonsilla	Low
6	M	59	T3N1M0	Tonsilla	Low
7	M	47	T4N3M0	Epipharynx	Low
8	M	64	T2N2aM0	Tonsilla	Low
9	M	18	T3N3M0	Epipharynx	Low
10*	M	45	T2N2bM0	Tongue base	High

M = male, F = female, diff = cell differentiation. * Patient No10 was excluded in Paper Ⅱ.

6.1.2 Prostate cancer patients (Paper Ⅲ)

Sixteen patients with rising PSA levels of biochemical recurrent prostate cancer who underwent a second folllow up C-AC PET-CT were included. The

PSA levels at the time of recurrence ranged from 0.3-51.0 ng/ml (median 5.2 ng/ml) after different treatment. The median Gleason sum was 7 (range 4 - 9). Patients clinic characteristics are shown in Table 2. Five patients were previously operated on with prostatectomy only, 6 were treated with RT only, 5 with a combination of RT and hormonal therapy.

Table 2 Patients clinical characteristics.

Patient No	Age	Gleason Sum	PSA* (ng/ml)	Treatment
1	61	7	4.4	O
2	71	7	7.3	RT+H
3	64	8	51.0	RT+H
4	72	7	0.6	RT+H
5	65	9	10.0	RT+H
6	69	7	0.8	O
7	57	6	0.3	O
8	77	7	15.0	RT
9	74	4	3.2	O
10	62	7	0.5	RT
11	60	5	50.0	RT
12	81	6	22.0	RT+H
13	66	4	3.9	RT
14	78	8	5.5	RT
15	74	7	4.8	O
16	72	6	37.0	RT
Range	57-81	4-9	0.3-51.0	
Median	70	7	5.2	

RT = Radiotherapy, H = hormonal therapy, O = operation. * = PSA level at the time of recurrence.

6.1.3 Animal studies (Paper Ⅳ)

Three female cynomolgus monkeys (*Macaca fascicularis*) weighing 6.6, 4.6, and 3.2 kg and one female domestic pig (*Sus scrofa*) weighing 12 kg were prepared according to a standard protocol before intubation and maintained on

artificial ventilation and sevoflurane inhalation anaesthesia (2-4%) throughout the study.

6.2 PET imaging protocols

6.2.1 FDG PET in head and neck cancer patients

Whole body FDG PET or PET-CT was performed at baseline 1 hour after intravenous injection of 5 MBq/kg body weight of FDG. The first scan was done from the thorax to the pelvic with the arm resting above the head; the second scan was done to cover head and neck area with the arms alongside of the body. Scan duration was 4min/bed for PET-CT and 5min/bed for PET alone.

6.2.2 C-AC PET in head and neck cancer patients

Dynamic C-AC PET were performed at baseline and during RT. Baseline C-AC PET were performed either on the same day of FDG PET or on the consecutive days. During RT, 5 patients were performed after a mean dose of 15Gy was delivered (range 9.6 - 20Gy), in 7 patients after a mean dose of 30Gy (range 24 - 37Gy) and in 8 patients after a mean dose of 55Gy (range 42 - 68Gy). In order to absolute quantification of the tumor perfusion, dynamic heart scan (n = 23) was acquired to derive artery input function in Paper Ⅱ. Scan protocol was 12×5s, 6×10s, 4×30s and 1×60s immediately started after bolus injection of 0.5MBq/kg body weight of C-AC. Ten minutes after the heart scan, dynamic head and neck tumor scan was performed directly after bolus injection of 10MBq/kg body weight of C-AC. The scan was composed of 12×5s, 6×10s, 4×30s, 4×60s, 2×120s and 4×300s frames within 32 min.

6.2.3 C-AC PET in prostate cancer patients

Dynamic C-AC PET-CT at prostate region were performed in 15 patients after injected 10MBq/kg body weight of C-AC. The total scan time was 8 min with time frames of 12×5s, 6×10s, 4×30s, 4×60s. Ten min after injection, whole body non-contrast helical CT scan with 140kV, 80mA was acquired followed by static PET imaging in all 16 patients. Scan was done from the thigh to the jugular notch with 4min/bed. Attenuation correction was performed by CT images. PET images were reconstructed by an iterative algorithm.

6.2.4 C-AC and F-AC PET in animals

Dynamic AC PET-CT scans (12x5s, 6x10s, 3x20s, 3x60s, 2x120s, 3x300s, 29 frames in 25 min) were performed to specifically evaluate the kinetics in the myocardium and liver. The injection dose were 68 ± 60 MBq of C-AC and 55 ± 33 MBq of F-AC in monkey and 219 MBq and 115 MBq in pig, respectively. Blood samples for radioactivity measurements in whole blood and plasma were taken at 0.5, 1, 2, 5, 10, 15, 25, 60, 90, and 120 minutes after each tracer injection. Serial whole body scans (4 beds, 5 min/bed) were performed at 30, 60, 90 and 120 min after tracer administration to evaluate distribution and retention of tracers in other metabolizing organs. An additional F-AC scan after injection 180min was performed in the monkeys.

6.3 PET imaging Analysis

6.3.1 Baseline FDG and C-AC PET in head and neck cancer patients (Paper Ⅰ)

Baseline FDG PET and C-AC PET images were coregistered with diagnostic CT/MRI and doseplanning CT. Frame 30 (images acquired after injection 17-22 min) of dynamic C-AC PET scan, usually provided the best tumor to background contrast and was selected for further analysis of detecting and delineating tumor volume in Paper Ⅰ. FDG and C-AC PET images were analyzed both qualitatively and semi-quantitatively with SUV. SUV was calculated by dividing the mean radioactivity of whole tumor volume (Bq/cc) with the per body weight(g) injection dose(Bq). Two physicians of nuclear medicine independently interpreted the images visually and in consensus. Tumor uptake of FDG and C-AC were graded into negligible, mild, moderate and intense according to the contralateral or surrounding tissues. Abnormal uptake equal to or exceeding the mild was deemed pathology.

6.3.2 Delineation of tumor volume (Paper Ⅰ)

Tumor volume was automatically delineated in 3 dimensional images in FDG PET and C-AC PET through tracing an isoradioactivity pixel value set to 50% threshold of the maximum radioactivity and corrected by the variable background

(Figure3). The background radioactivity was drawn from an adjacent tissue but safely separated from the tumor. The iosradioactivity pixel value was calculated as the equation:

Isoradioactivity pixel value = (*MPV*tumor + *APV*background) × 50%

Where *MPV* is the maximum radioactivity pixel value, *APV* is the average radioactivity pixel value of the background.

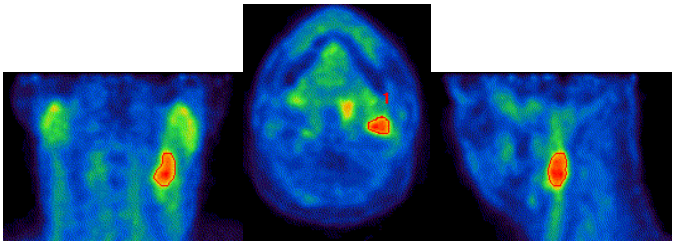

Figure 3 An example of tracing the isoradioactivity pixel value in 3 dimensions in one patient.

6.3.3 Serial dynamic C-AC PET (Paper Ⅱ)

6.3.3.1 Tumor clearance rate (k_{mono})

Time activity curve (TAC) of the primary tumor was obtained from a region of interest (ROI) delineating the highest uptake of tumor in all serial C-AC scans. TACs were analyzed by fitting an exponential curve to the data collected between 4 and 32 min (Figure 4). Tumor oxidative metabolism was derived from the slope of the equation below.

$$Y = Ae^{-kmono*t}$$

where Y is the tumor radioactivity (Bq/ml), A is a constant, t is time (min), and k_{mono} is the clearance rate of [^{11}C] in min^{-1}. The average R^2 of the fit was 0.93.

6.3.3.2 Tumor perfusion

The arterial blood input function was derived by placing a small ROI in the left ventricular cavity of the heart scan to obtain a TAC of the first pass of the bolus. Arterial blood activities were integrated by the area-under-the-curve of the first bolus passage through the chamber and normalized to the injected dose of the

subsequent tumor scan. Assuming that systemic circulation was unchanged between the heart and tumor scan.

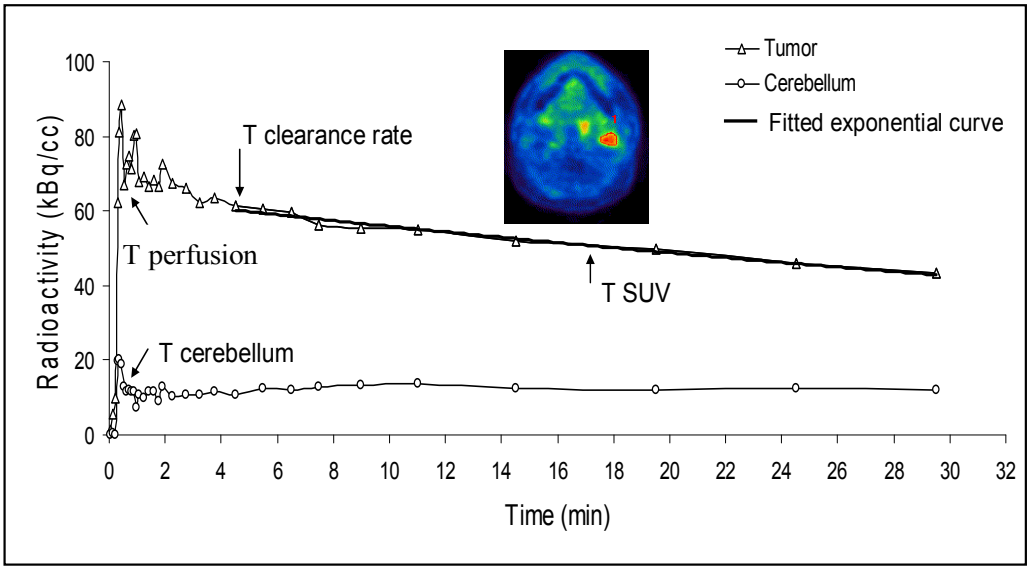

Figure 4 Time-activity curves from dynamic 1-[^{11}C]-acetate PET of the primary tumor and cerebellum in one patient. Arrows indicated time points where the radioactivity were measured. Inserted image was a transaxial slice representing [^{11}C] at the level of maximum tumor uptake (outlined) at 17 min post injection. T is the time of measurement. SUV is the standardized uptake value. Derived from Paper Ⅱ.

The absolute extraction rate (in ml/min per ml tissue) of primary tumor was calculated by dividing the first pass deposit in tumor by the arterial blood integral. As the arterial input was not obtained in all sessions, a relative perfusion index (rF) was quantified by the ratio of initial peak retention in the tumor to that of the cerebellum (Figure 4). The cerebellum was chosen as a reference because this region was excluded from RT and had a highly stable extraction rate in all patients with minimal variation in the serial scans. Absolute quantification of tumor perfusion was 0.47 ± 0.04 ml/min per ml tissue in 23 scans. The mean of simultaneous rF measurements was 5.87 ± 0.39 and the correlation between the results of the two methods was statistically significant ($p = 0.005$).

6.3.3.3 Tumor SUV

C-AC SUV of primary tumor was determined by the radioactivity concentration of the ROI which covered the highest tumor uptake dividing by the injected dose per gram body weight at 17–22min after injection (Figure 4). Tumor

glucose uptake (Tglu) expressed by FDG SUV using the same formula as for C-AC SUV.

6.3.3.4 RT and tumor response

External beam RT with standardized conformal techniques was delivered to the primary and lymphnode metastasis using 3D treatment planning. The total dose was 68Gy with 2Gy per fraction and 5 fractions per week. The treatment response of RT was evaluated 6-8 weeks after the completion of the RT by clinical examination, endoscopy and CT/MRI imaging according to the standard criteria [89]. Patients were followed up regularly according to the routines of the departments. The median follow up time was 33 months (range 26-46 months). Six patients were considered in complete response (CR), of which 5 were alive at the time of evaluation. One patient died of causes unrelated to cancer. Three patients had partial response (PR) and all died during the follow-up due to cancer progression.

6.3.4 C-AC PET in prostate cancer (Paper Ⅲ)

The PET-CT images were analyzed together by one radiologist and one nuclear physician. First, any lymph node and recurrence with C-AC uptake higher than in the surrounding or contralateral normal tissues, and displayed in three consecutive slices, was considered an abnormal lesion. Secondly, high uptake in superficial inguinal lymph nodes with CT Hounsfield unit (HU) <5 or bilateral symmetric high uptake nodes even with soft tissue density was considered benign. Abnormal lymph nodes were grouped into malignant lymph node (M-LN) and benign superficial inguinal nodes (B-LN) based on the follow up PET-CT scan. The mean CT HU, SUV maximum, size and the ratio of long to short axis (L/S)of each abnormal lymph node were evaluated. No M-LN was found in the first dynamic PET-CT scan covering the prostate region. Kinetic curves were therefore only available for B-LN and primary recurrences, and were obtained from the ROIs which covered the maximum uptake of the lesions for further analysis.

6.3.5 AC PET in animals (Paper Ⅳ)

In the dynamic studies, ROIs encompassing the left ventricular myocardium and liver were drawn using software developed in-house, and TACs were

exported for further analysis. In the whole body studies, ROIs were drawn in bone, brain, colon, fat, gallbladder, heart chamber, heart muscle, kidney, liver, lung, muscle, pancreas, salivary gland, small bowel, spleen, thymus, and bladder (urine) at several time-points. SUV were calculated for all regions. Total body and skeletal radioactivity retention were assessed from the whole-body studies at the 2 h time-point.

6.4 Statistics

Non-parametric Wilcoxon signed rank test was used for evaluating the differences of SUV, tumor volumes between FDG and C-AC PET (Paper Ⅰ).The differences of HU, SUV, size and L/S ratio between B-LN and M-LN in Paper Ⅲ were analyzed by Independent Sample T test. ANOVA test was used to analyze tumor rF, k_{mono} and SUV in the serial scans (Paper Ⅱ) and to compare tumor uptake with histological cell diferentiation. Non-parametric Wilcoxon Mann-Whitney U test was used to analyze the differences between CR group and PR group. The relationship of k_{mono}, rF and Tglu was determined by Spearman's correlation coefficient. P value less than 0.05 was considered significant.

7 Results and Discussion

7.1 Detecting primary tumors and lymph node metastases

7.1.1 Primary tumors (Paper Ⅰ)

Accurate diagnosis and staging tumor before therapy are crucial for treatment scheme and prognosis. In this ten patients study, all the primary tumors were detected by C-AC PET. Nine of 10 tumors were identified by FDG PET and CT/MRI respectively (Table 3, Figure 5). In patient 10, the primary tumor in the left base of tongue was missed both by FDG PET and CT, but clearly visualized by C-AC PET (Figure 6). FDG SUV tended to be higher than C-AC SUV. Neither C-AC SUV nor FDG SUV correlated with the histopathological grade.

Table 3 Qualitative and semi-quantitative analysis of C-AC and FDG PET for primary tumors.

Patient	C-AC-PET			FDG-PET		
	SUV	Visual	Volumes (cc)	SUV	Visual	Volumes (cc)
1	9.2	+++	9.5	13.5	+++	3.1
2	2.5	+	3.9	3.8	++	3.4
3	6.0	+++	8.6	24.5	+++	6.0
4	2.7	+	24.6	4.4	++	13.0
5	5.7	+++	17.5	12.9	+++	10.1
6	3.8	++	15.0	7.9	+++	10.5
7	10.6	+++	4.7	6.7	+++	5.3
8	4.9	++	1.8	4.7	++	1.5
9	3.9	++	15.1	15.4	+++	13.5
10	3.7	++	1.8	1.9	-	¤
Mean ± SD	5.3 ± 2.7		11.2 ± 7.4	9.6 ± 7.0		7.4 ± 4.5

SUV = standardized uptake value; - = negligible uptake, + = mild uptake, ++ = moderate uptake, +++ = intensive uptake; SD = standard deviation; ¤ = not measurable.

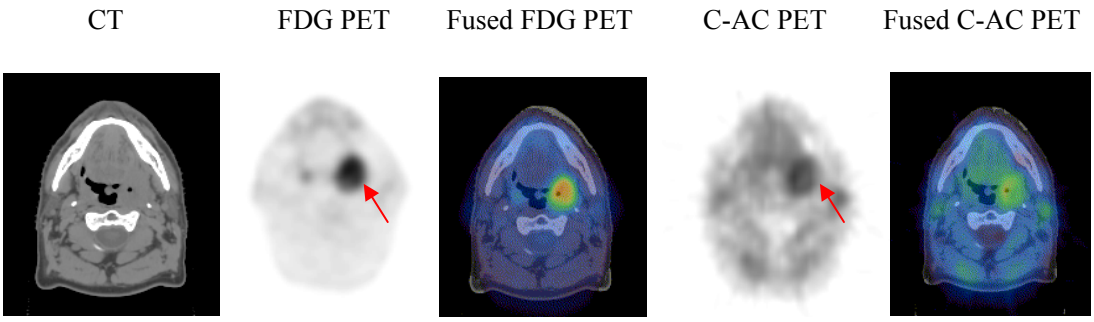

Figure 5 Patient No 6 with squamous cell carcinoma in left tonsil. The tumor exhibited increased uptake of FDG (SUV 7.9) and C-AC (SUV 3.8) (arrows). Derived from Paper Ⅰ.

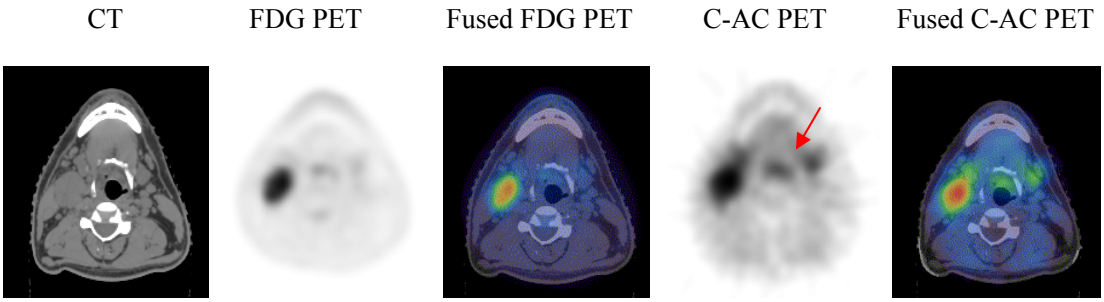

Figure 6 Patient No 10 with squamous cell carcinoma in left base of the tongue and metastases at the right side of the neck. C-AC-PET clearly exhibited high uptake in the primary tumor with SUV 3.7 (arrow). However, FDG failed to show a significantly increased uptake with SUV only 1.9 and missed the primary tumor. CT has also showed a false negative result. All of the images showed the contralateral lymph node metastasis. Derived from Paper Ⅰ.

7.1.2 Lymph node metastases (M-LN) (Paper Ⅰ)

Total 21 M-LN were found in 7 patients. Almost all 20/21 M-LN were detected by C-AC PET, but only 13/21 M-LN were detected by FDG PET (Table 4), and 16/21 M-LN were detected by CT/MRI. Only 1 metastasis which had a small volume 0.8cc missed by C-AC PET, but visualized by FDG PET (SUV3.8). In patient No10, four M-LN were false negative both in FDG and CT, while all of them were identified by C-AC (Figure 7). There are no differences and correlations of C-AC SUV 4.0 ± 1.3 (2.4 - 6.2) and FDG SUV 4.5 ± 3.3 (0.9-10.0).

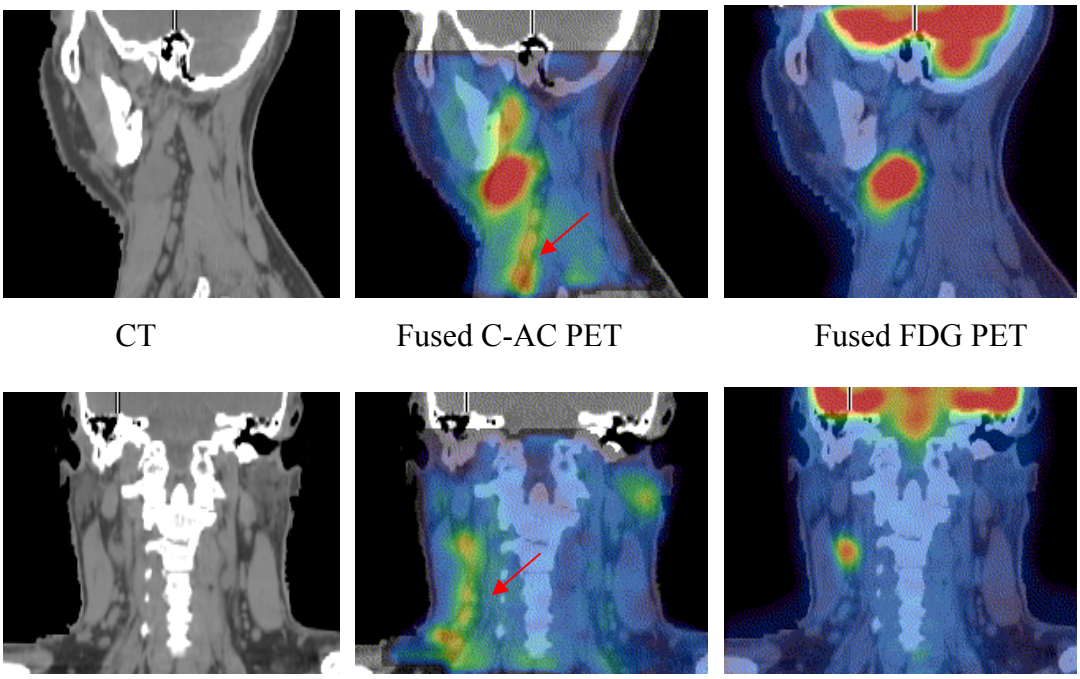

Figure 7 Patient No 10 with squamous cell carcinoma in left base of the tongue and clustered metastases at the right side of the neck. The largest lymph node metastasis was visualized by both FDG and C-AC PET. But only C-AC PET detected the clustered lymph node metastases with high uptake in the right side of the neck (arrows). CT and FDG missed these multiple metastases.

C-AC PET seemed more sensitive than FDG PET for detecting both the primary tumors and metastases in head and neck SCC. The missed primary and metastases by FDG PET might be caused by the faint uptake of FDG in well differentiated tumor [90]. Further, this kind of tumor might predominantly depend on oxidative metabolism for their bioenergetic needs rather than glycolysis. Equal to FDG, high physiologic uptake of C-AC was also found in the salivary gland, tonsil, and sometimes muscle, leading to lower contrast of tumor to background and potentially false negative results in these regions. One small lesion missed by C-AC PET was obscured by the high uptake of the adjacent salivary gland. Fused PET images with the anatomic information or the use of PET-CT may overcome this shortcoming. The uptake mechanism of C-AC in tumor remains unclear, probably due to the accelerated anabolic pathway mixed with the enhanced lipid and amino acid synthesis [54].

Table 4 Qualitative and semi-quantitative analysis of C-AC and FDG-PET for metastases.

Patient	No of Metastases	C-AC-PET			FDG-PET		
		SUV	Visual	Volumes (cc)	SUV	Visual	Volumes (cc)
1	1	5.9	+++	1.2	1.5	-	¤
	2	5.9	+++	2.2	5.2	+++	1.4
	3	5.9	+++	1.8	5.4	+++	0.8
	4	4.7	++	1.9	4.9	++	1.7
5	1	5.1	+++	101.0	13.0	+++	82.4
	2	3.1	++	1.4	3.8	++	1.7
6	1	2.9	++	1.4	3.6	++	1.2
7	1	4.5	++	1.5	1.7	-	¤
	2	3.9	++	1.5	1.3	-	¤
	3	4.6	++	1.7	1.5	-	¤
8	1	5.8	+++	4.6	7.6	+++	3.9
9	1	3.0	-	¤	3.8	++	0.8
	2	2.8	+	1.8	6.4	+++	1.5
	3	2.6	+	3.5	6.2	+++	2.9
	4	3.7	++	14.5	8.1	+++	13.2
	5	3.0	++	4.8	5.7	+++	3.7
10	1	6.2	+++	14.5	10.0	+++	10.5
	2	2.4	+	1.1	1.1	-	¤
	3	2.6	+	1.6	1.2	-	¤
	4	2.7	+	0.8	0.9	-	¤
	5	3.5	++	1.8	1.0	-	¤

SUV = standardized uptake value; - = negligible uptake, + = mild uptake, ++ = moderate uptake, +++ = intensive uptake; ¤ = not measurable. The median volumes of the metastases drawn by C-AC were 2.9 ± 10.3cc, compared to 2.3 ± 7.4cc when FDG was used.

7.2 Delineating tumor volumes

FDG PET has been widely accepted as a complementary tool in delineating gross tumor volume in RT dose planning. It provides distinctive biologic information and facilitates the optimal individualized RT. Integrated PET and CT volumes improve the tumor definition and avoid unnecessary irradiation in surrounding normal tissues, therefore providing a chance for dose escalation and reduction of normal tissues complications. However, there are few reports on C-AC PET for delineating the gross tumor volume. In Paper Ⅰ, the mean primary tumor volumes delineated by C-AC PET and FDG PET were 11.2 ± 7.4cc (1.8-24.6cc) and 7.4 ± 4.5cc (1.5-13.5cc) respectively (Table 3). Eight of 9 tumor volumes delineated by C-AC PET were larger than that in FDG PET, except 1 volume that was slightly smaller. The mean tumor volumes derived by C-AC PET were 51% larger than that of FDG PET (p = 0.02) (Figure 8). Especially in patient No1, tumor volumes of C-AC were three times larger than that of FDG, almost two times larger in patient No 4 and No 5. Volumes of metastases delineated by C-AC PET (2.9±10.3cc) were also 23% larger (p = 0.005) than the volumes derived from FDG PET(2.3±7.4cc) (Table 4).

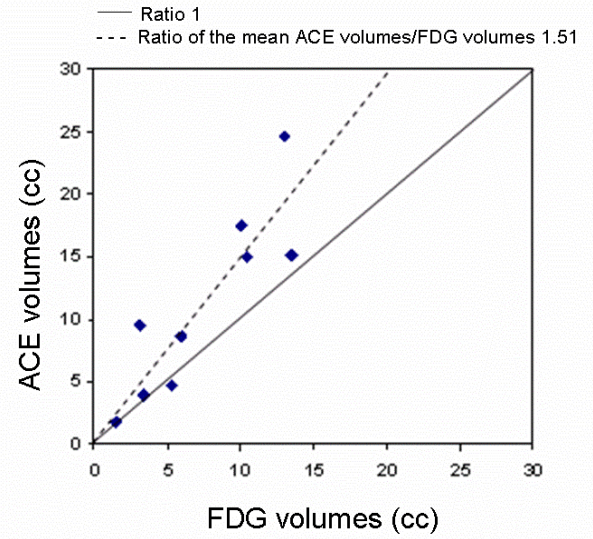

Figure 8 Ratios of C-AC volume to FDG volume, 8 of 9 ratios exceeded unity. Derived from Paper Ⅰ.

The interesting and important findings were the large differences between C-AC volumes and FDG volumes. It immediately raises several questions: Whether FDG PET accurately delineated tumor volumes? Should an extra 51% volume delineated by C-AC PET be irradiated for an additional dose regimen? High uptake of both tracers located at different part of certain tumors has been found in HCC [46]. Kaji et al [91] also reported that high C-AC uptake covered well and moderate differentiated lung adenocarcinoma, while FDG only encompassed the moderated differenciated component of the tumors. As heterogeneity is one of the main characters of cancer, the C-AC volumes larger than FDG volumes observed in the current study are probably due to C-AC additionally outlining the relatively well differentiated infiltrated tumors which are not FDG avid. More studies comparing with golden standard histopathological tumor volumes are needed.

PET imaging with different tracers, such as FDG, ^{11}C-methionine, ^{18}F - fluoromisonidazole have substantially impacted in RT planning [92]. None the less, the definition of metabolic tumor volumes remains challenging, as there is no consensus concerning the optimal method for segmenting the metabolic activity lesions. Different methods may obtain different results [93]. Manual delineation has a high inter-observer variation and are less reproducible [94]. Automatically outlining tumor volume with threshold set to the maximum radioactivity is often used clinically. SUV >2.5 or 50% threshold appears more practical in lung cancer and head and neck cancer [95, 96]. However, it might be compromised by the significant heterogeneous uptake of tumors and high uptake of surrounding tissues. It is difficult to find a cutoff value fitting all the tumors in a clinical setting, especially in the head and neck region with complex structures and heterogeneous tumor metabolism. Volume delineating in this study established a new development in this field. Our method outlined 50% threshold of maximum radioactivity with the consideration of the variable background radioactivity and appeared to be both fast and reproducible. The intensity level representing the actual radioactivity distribution of the tumor and depends on many specific factors. The only factor influences the reproducibility is the determination of the background radioactivity, which results in only a few percent variation. Tumor volume delineation based on

texture features which were extracted from corresponding PET-CT images also appeared promising [97].

7.3 Tumor oxidative metabolism during RT

Tumor oxidative metabolic rates (k_{mono}) (mean± SE) in **Paper Ⅱ** are presented in Table 5 and Figure 9. Before RT, k_{mono} of CR was almost double to that of PR ($p = 0.02$) and did not change significantly during RT. This indicates that tumors with high radioresponsiveness rely predominantly on cellular respiration for energy formation during RT. In contrast, the k_{mono} of PR was significantly increased at 30 Gy ($p = 0.002$) and 55 Gy ($p = 0.008$), compared to baseline, suggesting that mitochondrial dysfunction in radioresistant tumors is reversible. Treatment targeting on the intermediate metabolism might improve the patient outcome. Only one patient was scanned at 15 Gy in PR and therefore not included in the ANOVA analysis. k_{mono} was not significantly different between CR and PR at 30 Gy or 55 Gy.

This is the first time that C-AC PET was used to image tumor oxidative metabolism and the link of bioenergetics towards radioresistance in patients. Oxidative metabolism was assessed by calculating the monoexponential clearance rate k_{mono} of [^{11}C] from tissue by a simple fitting procedure. This method is based on the assumption that radiolabeled acetate reaches the mitochondria with the formation of ^{11}C-Acetyl CoA and is terminally oxidized to [^{11}C]-CO_2 which is exhaled from the lungs, causes a diminishing tumor radiosignal in the PET images (Figure2). Similar techniques using [^{14}C]-labeled substrates of the intermediary metabolism have been available for decades in vitro. Notably, k_{mono} of C-AC PET is the golden standard for non-invasive measurement of regional cardiac oxygen consumption and was recently also validated in a renal animal model [58, 98]. k_{mono} values in cancers measured in this study were substantially lower than that of myocardium in resting normal volunteers (0.05-0.07 min^{-1}) [83]. Whether k_{mono} from different tissues are directly comparable remains unknown. On the other hand, unlike myocardium, lipogenesis is upregulated in several cancer types. Variable [^{11}C]-Acetyl-CoA might be activated by cytosolic enzymes ACS1 for lipid formation in cancer cells leading to a amount of radioactivity in cytosol and potentially lowering the clearance rate.

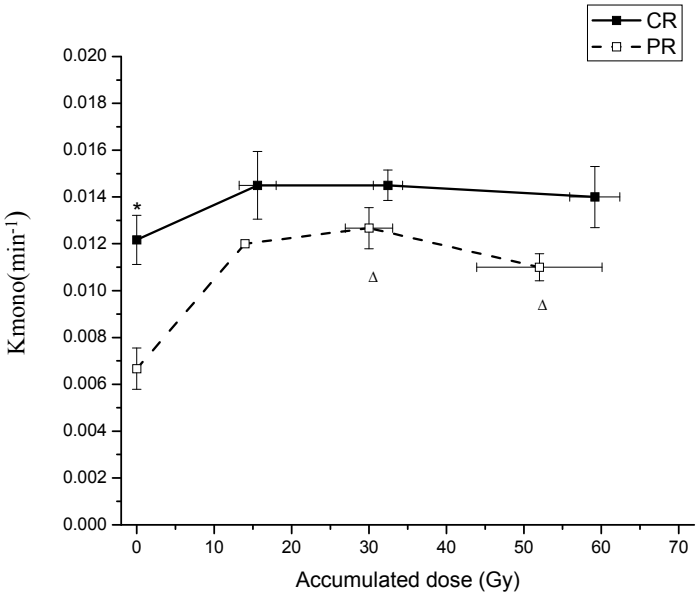

Figure 9. Changes in the oxidative metabolic rate (k_{mono}) (mean± SE) of the primary tumors during RT in complete (CR) and partial responders (PR). * indicates significant difference of k_{mono}between CR and PR at baseline (p = 0.02). Δ indicates significant increase of k_{mono} from baseline to 30 Gy and 55 Gy in PR (ANOVA p = 0.004). Derived from Paper Ⅱ.

Table 5 Oxidative metabolic rate (k_{mono}, unit min^{-1}) of primary tumor in each patient during RT.

TR	Patients	Baseline	15Gy	30Gy	55Gy
CR	1	0.0115	ND	ND	0.0127
CR	2	0.0121	0.0178	0.0145	0.0181
CR	4	0.0097	0.0109	0.0130	0.0143
CR	6	0.0124	ND	0.0136	0.0097
CR	7	0.0173	0.0146	ND	ND
CR	8	0.0099	0.0135	0.0164	0.0153
Mean ± SE		0.0122 ± 0.0011	0.0142 ± 0.0015	0.0144 ± 0.0008	0.0140 ± 0.0014
counts of scan		6	4	4	5
PR	3	0.0051	ND	0.0128	0.0120
PR	5	0.0078	ND	0.0109	0.0104
PR	9	0.0065	0.0116	0.0140	0.0105
Mean ± SE		0.0065 ± 0.0008	ND	0.0126 ± 0.0009	0.0110 ± 0.0005
counts of scan		3	1	3	3

TR = tumor response; CR = complete response; PR = partial response; ND = no data available

Baseline Tglu of all primaries expressed by FDG SUV was 10.9 ± 2.4 (mean±SE) ranged 3.9 - 26.1 in **Paper Ⅱ**. Tglu was significantly higher in PR than that in CR patients (p = 0.04). This further imply that tumor radioresistance is predominantly dependent on glycolysis for bioenergetic needs. An inverse tendency was found between Tglu and k_{mono} at baseline (r = -0.57, p = 0.11) (Figure10). This suggests there exist a bioenergy switch from oxidative metabolism to glycolysis.

There are several different mechanisms by which cancer cells might develop a poor bioenergetic metabolism - glycolysis. Mitochondrial DNA mutations [99], hypoxia [100], altered regulation of enzymes in both bioenergetic pathways and accelerated proliferation [12, 101, 102] are all associated with this bioenergetic switch. Most likely, this phenotype facilitates cell survival either by minimizing oxygen dependence or by downregulating the pro-apoptotic role of mitochondria. Recent study indicated that forcing tumor cells from glycolysis back into mitochondrial oxidative metabolism inhibited cancer growth and postulated that tumor invasiveness might be inversely linked to cellular respiration [103]. This is in accordance with our findings. Our data translates the previous findings of tumor bioenergy metabolism from in vitro into the clinical situation. Quantitative metabolic imaging might open a new method for investigating tumor bioenergetics in patients.

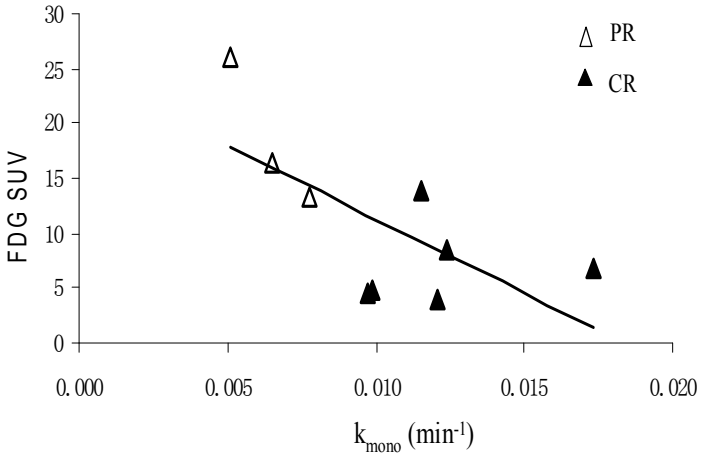

Figure10 Correlation of clearance rate (k_{mono}) and glucose uptake expressed by FDG SUV of primary tumors at baseline. The k_{mono} tended to correlate inversely with glycolysis.

7.4 Tumor perfusion during RT

Table 6 and Figure 11 describe the related perfusion index (rF) (mean± SE) of the primary tumor of CR versus PR in **Paper Ⅱ**. In the CR group, tumor rF tended to increase from baseline to 15 Gy (p = 0.06), was relatively stable at 30 Gy and then decreased at 55 Gy (p = 0.03, compared with the rF at 15 Gy). This finding fits well with the concept that cell death early during successful RT causes tumor decompresssion, leading to reperfusion [104]. At the end of therapy, when most tumor cells were killed, total metabolic demand was reduced and less perfusion was needed. No significant changes of rF were observed in PR (p = 0.41). No difference of rF between CR and PR at the same doses was found.

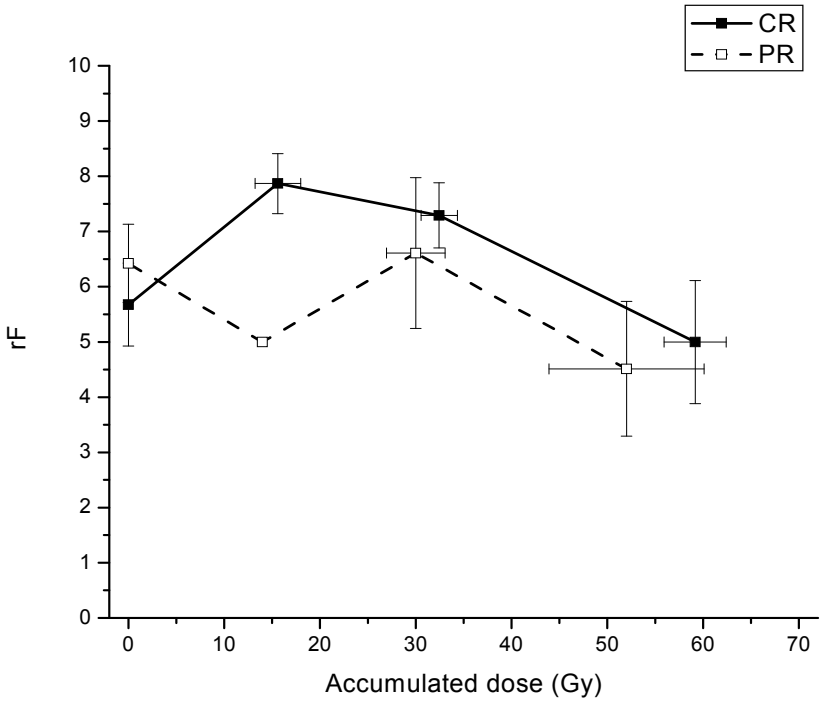

Figure 11. Changes in the relative perfusion index (rF) (mean± SE) of the primary tumors during RT in complete (CR) and partial responders (PR). No significant differences were found between the two groups during RT. Derived from Paper Ⅱ.

Kinetic estimation of perfusion using PET requires a blood input function from true arterial samples or from a substantial blood compartment in the image. Arterial sampling was deemed too invasive in this study and intravascular activity in neck vessels can not be accurately measured by PET, due to partial volume

effects. Therefore we assessed arterial C-AC activity from near simultaneous left ventricular blood pool imaging, a standard method in quantitative perfusion in cardiac PET. Absolute C-AC extraction rate averaged 0.47 ml/min per ml tissue, approaching the perfusion rate recorded in healthy myocardium at rest using the same technique and that of previous data in human cancers using other methods [105]. Although this approach is noninvasive, it added to the complexity of the study. Dynamic cardiac scans were not obtained at all time points for logistic reasons. Substituting blood activity with a cerebellar reference successfully accomplished a simple index of nutritive tumor perfusion. Reports on tumor perfusion during treatment in vivo are scarce and somewhat contradictory [104]. Perfusion was similar for CR and PR in the present study and apparently not correlated to tumor response.

Table 6 The relative perfusion index (rF) of tumor in each patient during RT.

TR	Patient	Baseline	15Gy	30Gy	55Gy
CR	1	6.26	ND	ND	2.81
CR	2	4.90	8.22	8.06	7.76
CR	4	3.96	7.07	6.54	ND
CR	6	5.91	ND	6.05	3.64
CR	7	8.93	9.25	ND	ND
CR	8	4.10	6.93	8.51	5.78
Mean ± SE		5.68 ± 0.75	7.87 ± 0.54	7.29 ± 0.59	5.00 ± 1.11
counts of scan		6	4	4	5
PR	3	7.63	ND	7.39	5.00
PR	5	6.47	ND	8.48	6.34
PR	9	5.17	5.00	3.95	2.20
Mean ± SE		6.42 ± 0.71	ND	6.61 ± 1.37	4.51 ± 1.22
counts of scan		3	1	3	3

TR = tumor response; CR = complete response; PR = partial response; ND = no data available due to the technique problem or patient absence.

7.5 Correlations of tumor oxidative metabolism, perfusion and glycolysis

C-AC PET provided quantitative assessment of nutritive perfusion and oxidative metabolism. A positive correlation of overall k_{mono} and rF was found in the CR ($r = 0.72$, $p = 0.001$, $n = 18$) (Figure 12A). This correlation was even better at baseline ($r = 0.83$, $p = 0.04$, $n = 6$). rF was highly coupled to the oxidative metabolic rate only in cancers with favorable outcome throughout the RT. This is in accordance with the tissues under normal physiology that regional perfusion is dictated by tissue demand. While k_{mono} and rF were not correlated in PR (Figure 12B).

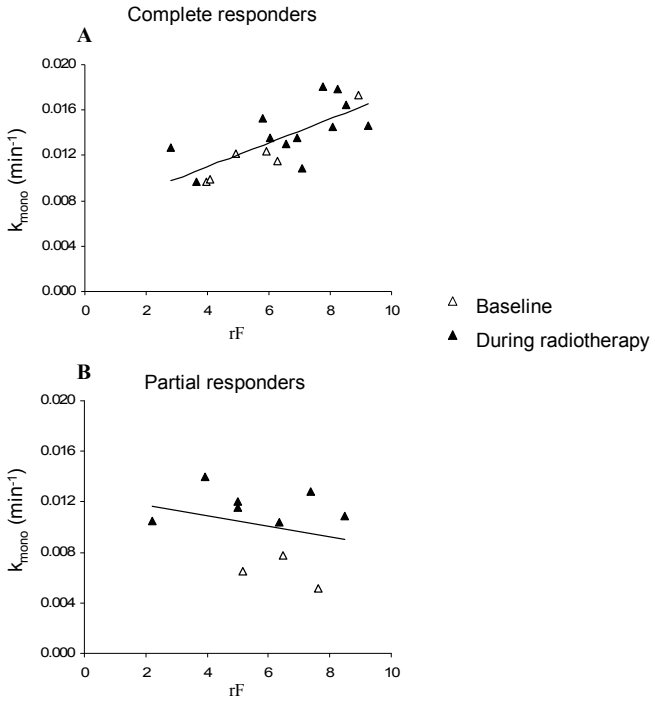

Figure 12. Correlation between the oxidative metabolic rate (k_{mono}) vs relative perfusion index (rF) of the primary tumors in complete responders (CR) in panel **A** and partial responders (PR) in panel **B**. A positive correlation of the overall k_{mono} and rF was found in the CR group. k_{mono} and rF were not correlated in the PR group. Derived from Paper Ⅱ.

Baseline Tglu tended to correlate inversely with k_{mono} ($r = -0.57$, $p = 0.11$), but was not significantly correlated with rF. Further, rF of CR and PR was comparable throughout the RT. In despite of the intense perfusion, impaired oxidative metabolism increased during RT in PR tumors. This implies that the

increased oxidative metabolism in PR might not be explained by the reoxygenation from decompression and reperfusion alone and possibly resulted from the recovery of deranged mitochondria function.

7.6 Tumor C-AC SUV during RT

In **Paper Ⅱ**, no changes of tumor C-AC SUV in CR and PR during the treatment are shown in Figure 13. Differences of SUV between CR and PR at the same doses were also not found. Mean SUV was presented in this study, but results were similar when SUV maximum was used. Oyama et al [106] using C-AC PET to evaluate the metabolic changes in prostate cancer during the androgen ablation in an animal study, no SUV changes were found before and after treatment, similar to our findings. SUV measures tumor uptake at a certain time point after injection; therefore it does not trace the kinetics associated with radioresponsiveness. Furthermore, the retention of C-AC radioactivity is affected both by tumor perfusion and oxidative metabolism and seems to correlate minimally with enhanced lipogenesis in head and neck cancer. SUV changes might occur in relative long time span. The use of SUV alone for analyzing the C-AC PET imaging might compromise the meaningfulness of this tracer in oncology application.

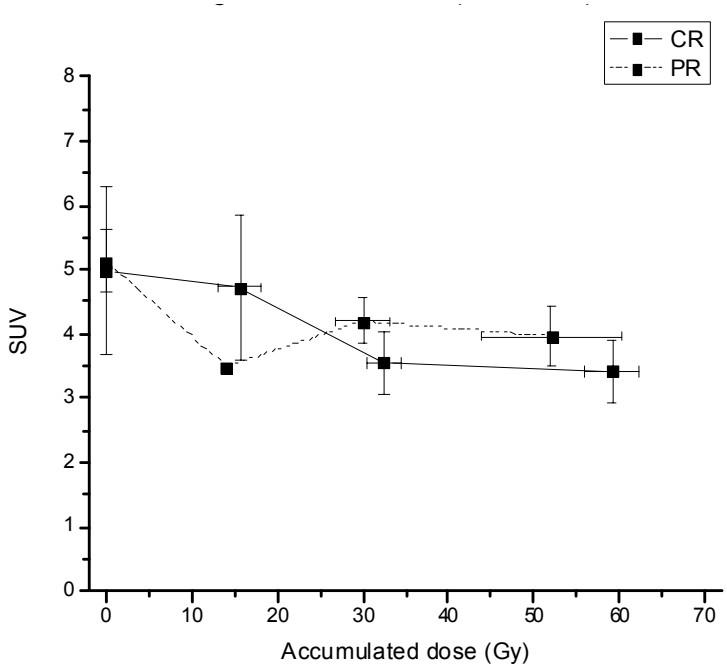

Figure 13 No changes of tumor SUV in patients with CR vs PR in the serial scans.

We propose a new non-invasive method for simultaneous assessment of head and neck tumor perfusion and oxidative metabolism in patients using dynamic C-AC PET. This method involves a single tracer injection, a short scanning protocol and simple evaluation techniques. It was used to document a bioenergy pattern that might predict radioresponsiveness. Restoration of tumor oxidative metabolism might be a potential target for improving the outcome in cancer therapy. The main limitation of this study was the small sample sizes and larger cohort studies are needed to confirm our findings.

7.7 SUV, CT HU of B-LN and M-LN in prostate cancer

Nodal staging in prostate cancer plays an major role for determining treatment scheme and prognosis. Patients with M-LN are considered incurable and 5-year disease free survival is poor [107]. The choice of treatment after biochemical relapse in patient depends on local recurrence and/or metastatic disease. Therefore, characterizing B-LN and M-LN is crucial for accuracy treatment. In **Paper Ⅲ**, a total of 30 lymph nodes with elevated C-AC uptake were identified in 12 patients. Eighteen B-LN in 8 patients and 12 M-LN in 8 patients respectively. Only 4 M-LN with the size more than 10mm. The mean HU and SUV of B-LN were significantly lower than those of M-LN ($p = 0.002$ and $p<0.001$, respectively) (Figure 14A and Figure 14B), but with considerable overlap in SUV. In the SUV overlapping group (SUV 3 - 5), both size and ratio of L/S were also similar (Figure 15A and Figure 15B). But the mean CT HU of B-LN (1.3 ± 7.2) was significantly lower than that of M-LN (28.0 ± 12.0) ($p<0.001$), (Figure 15C and Figure 16). Using a CT HU with cut-off value 15 would increase the specificity of C-AC PET-CT. However, some benign nodes have normal soft tissue density and small nodes should be evaluated with great care.

Initial M-LN of prostate cancer frequently occur in the obturator/internal iliac region (60-80%), followed by the external iliac region (20-25%). The presacral/presciatic/perirectal regions account for 14-15%, while 4% are found in the common iliac region [72, 73, 75, 108, 109]. The superficial inguinal region is

rarely involved. Given this background information and the results of the follow up scans in the this study, the B-LN were considered truly benign lymph nodes.

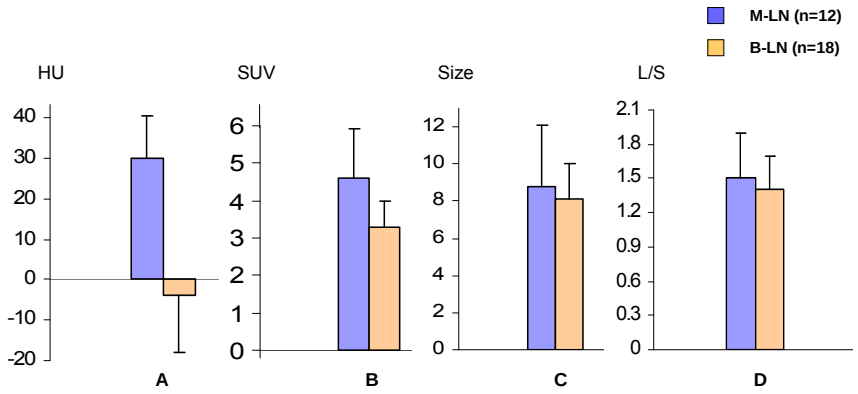

Figure 14 CT HU, SUV, Size and L/S ratio of M-LN and B-LN (mean±SD) of C-AC PET-CT in prostate cancer. The mean HU (A) and SUV (B) of M-LN were significantly higher than that of B-LN ($p<0.001$ and $p = 0.002$, respectively). No differences of size (C) and L/S ratio (D) between B-LN and M-LN were found. Derived from Paper Ⅲ.

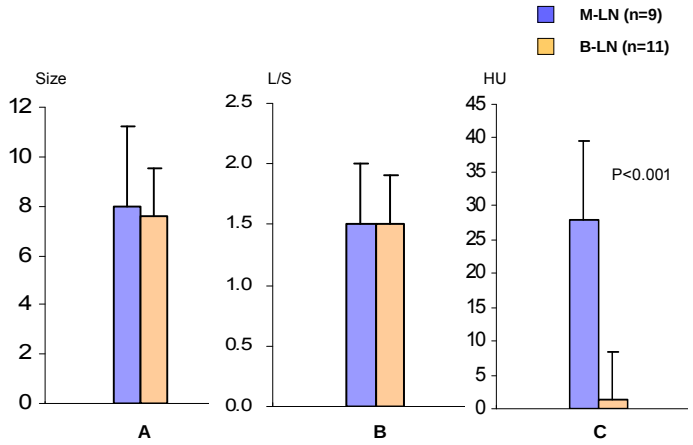

Figure 15: A huge difference of CT HU (mean±SD) between M-LN and B-LN of prostate cancer was shown in SUV (mean 3.8, range 3.0-5.0) overlapping group of C-AC PET-CT (C) ($p<0.001$). Both size (A) and L/S ratio (B) of M-LN and B-LN were comparable. Derived from Paper Ⅲ.

7.8 Kinetics of C-AC PET in B-LN and recurrent prostate cancer

Local recurrences were detected in 4 patients. Kinetic curves of the mean radioactivity in B-LN and local recurrences are shown in Figure 17. The radioactivity of both B-LN and recurrence peaked within the first few minutes. In

B-LN, less than 30% of the peak radioactivity was retained 8 minutes after injection. While the retention of local recurrences was almost 80% at the end of the dynamic scans. Unfortunately, no M-LN was included in the regional dynamic scan.

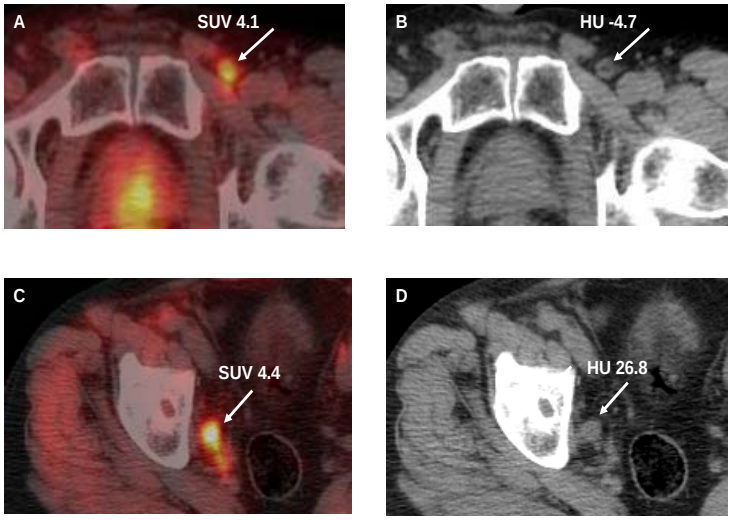

Figure 16 SUV and HU of B-LN (top) and M-LN (bottom) C-AC PET-CT in prostate cancer patient No9 and No16 respectively. Increased SUV of B-LN (A) was similar to M-LN (C), however, there is a quite low HU of B-LN (B) compared to M-LN (D). Derived from Paper Ⅲ.

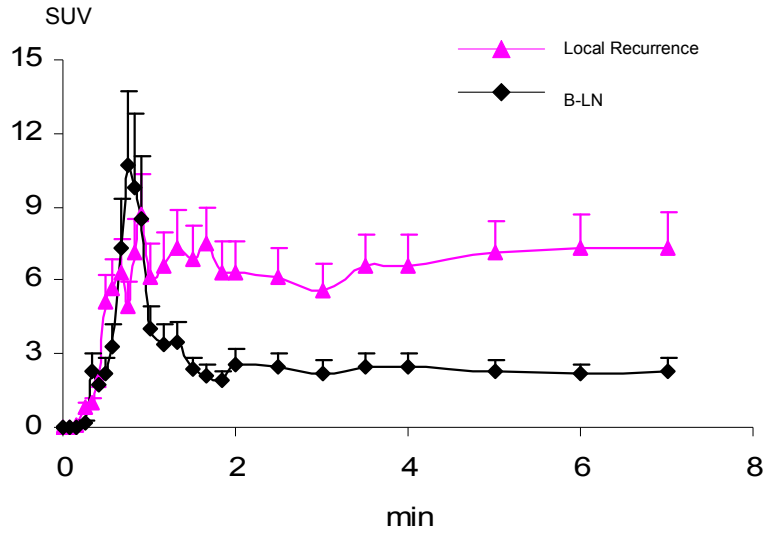

Figure 17 The kinetic curves (mean±SD) of the B-LN and local recurrent prostate cancer of C-AC PET-CT. Both B-LN and local recurrence have the equal high arterial perfusion in the first few minutes after injection. While compared with recurrence, less than 30% extraction of peak C-AC of B-LN entered into lipogenesis. Derived from Paper Ⅲ.

High C-AC uptake in prostate cancer is associated with an over expression of the enzyme FAS [71]. The mechanism of high C-AC uptake in fat-containing benign lymph nodes remains unknown. It could be caused by the passive lymph drainage containing ^{11}C-metabolites from the extremities or by lipogenesis as in cancers. If the former was the reason, dynamic imaging would be relevant to include into a clinical protocol. However, the kinetic analysis indicated that B-LN had equal high arterial perfusion as in the local relapses, suggesting C-AC retention in B-LN is solely associated with uptake from the blood stream. Combined with the increased lipid content in B-LN, as defined by CT, the finding suggests that C-AC retention is related to lipid formation and that fatty degeneration as a process involves an uncoupling of lipogenesis from metabolic needs. This seems to be in accordance with the proposed mechanism of C-AC uptake in prostate cancer [55] and further indicates that focally elevated lipogenesis is not a cancer-specific phenomenon.

Lymph node fatty degeneration can occur in any lymph node, but is frequently found in mesentery, groin and axilla. In this study, we also found five fatty degenerated nodes with elevated C-AC uptake in the axilla, data not shown. Fatty degeneration is usually observed in elderly persons and the incidence appears to increase gradually with age. It is caused by the infiltration of hyperplastic fatty tissue from the nodal hilus into cortex and finally resulting in lymph tissue atrophy [110]. Early in process of degeneration nodal lipid content is relatively low and morphology is not characteristic, as was the case in the majority of the B-LN investigated here. Most likely, there are other causes of increased nodal uptake needed to consider apart from prostate cancer metastasis and fatty degeneration, such as inflammation.

Dynamic C-AC PET ruled out the lymph drainage as the cause of high uptake in B-LN, probably being the increased lipogenesis. Combination of density measurement from CT HU might improve the specificity of nodal staging in prostate cancer. The small size of M-LN and all B-LN might have underestimated the HU and SUV due to the partial volume effect, which might limit the reproducibility of the quantitative parameters analyzed in this study.

C-AC PET appears promising both in head and neck cancer and prostate cancer. However, wider use of C-AC PET is restricted to sites with an on-site cyclotron due to the short half-life of carbon-11. Deveoping a ^{18}F-labeled variant of acetate therefore appears relevant.

7.9 Normal distribution of C-AC and F-AC in animals

7.9.1 Dynamic AC PET studies in blood, myocard and liver

To extend the clinic application of C-AC PET, in **PaperⅣ**, a novel tracer of F-AC was synthesized and used to evaluate the potential of F-AC as an analogue of C-AC for tracing carbon flux in the normal animal physiology. In venous blood, the concentration of ^{18}F decreased slowly and reached 4.0±1.4 SUV after 5 min, decreasing further to 2.4±0.84 SUV after 120 min in all animals. Meanwhile, the concentration of ^{11}C decreased rapidly and reached minimum at 0.8±0.13 SUV in monkey, 0.4 SUV in pig after 5 min. C-AC was rapidly cleared from the circulation, resulting in high initial retention in organs with high basal metabolism, except brain. The results corresponded with the pharmacodynamics and distribution of C-AC in man. The fractional extraction of acetate is approximately 70% both on the whole-body level and in individual organ systems [77, 78]. The high extraction therefore makes C-AC useful as a 'chemical microsphere' for PET and early imaging is primarily indicative of regional nutritive perfusion. In contrast to C-AC, F-AC had a much longer half-life in blood and no signs of specific retention. This indicates that F-AC does not behave as a chemical microsphere and therefore negates the usefulness of F-AC as a general perfusion tracer in PET imaging.

In myocardium, significant differences in the metabolic fate were observed in the exogenously supplied acetates. C-AC uptake rapidly reached a maximum during the first minute after injection in all animals, and followed by monoexponential clearance (Figure 18A). The early clearance rate of carbon-11 measured from 4 to 8 min after injection was 0.092 ± 0.023 min^{-1} in monkey and 0.083 min^{-1} in pig, reflecting oxidative metabolism. However, F-AC uptake was indistinguishable from the background activity in the blood throughout the study in all animals, and the TAC resembled those of blood (Figure 18A). In the

myocardium, the acetates are mainly activated by ACS2 in the mitochondria and used for combustion. Previous PET studies in humans have shown that approximately 80% of extracted C-AC is oxidized for combustion in proportion to myocardial oxygen consumption. The oxidized rate is easily measured by fitting a monoexponential TAC of early clearance from dynamic PET images. The rapid clearance in this study was approximately 10% per minute in both species. In contrast to C-AC, the retention of F-AC demonstrate that F-AC is not a preferred substrate for MCT, and minimal F-AC is converted to [^{18}F]-Acetyl-CoA. Indicating that F-AC is not useful tracer of ACS2 activity and therefore not indicative of mitochondrial function. F-AC was not related to intermediary oxidative metabolism.

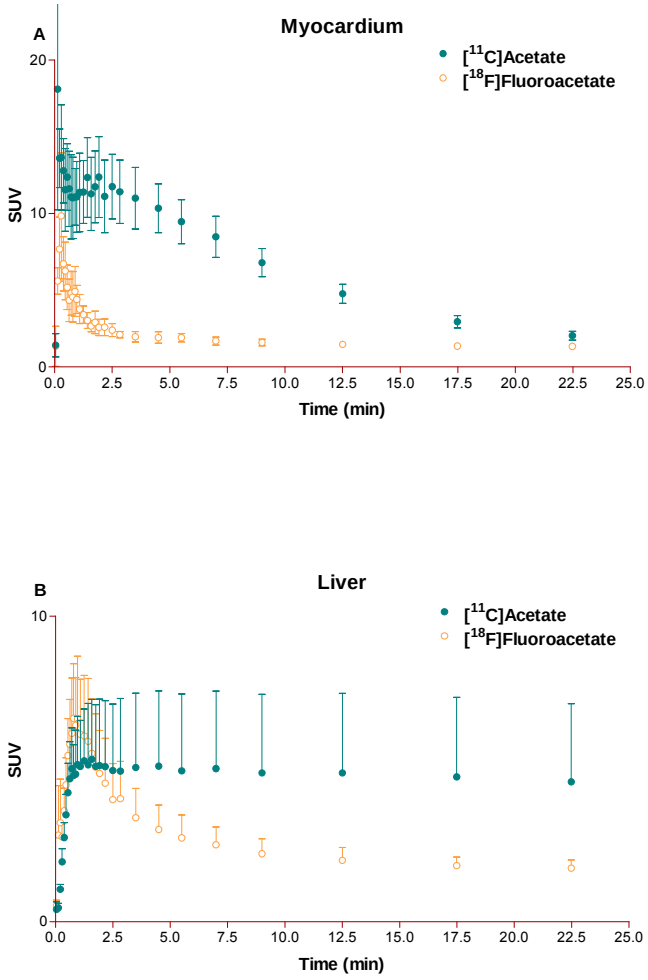

Figure 18 Plot of time-activity curves (mean±SE) in monkey from ROIs in Left ventricular myocard (**A**) and Liver (**B**). Significant difference between two compounds was observed in left ventricular myocard. While no difference between compounds in liver, probablely due to difference nutritional status among the monkeys. Filled dots: 1-[^{11}C]Acetate. Circles: 2-[^{18}F]fluoroacetate. Derived from Paper Ⅳ.

^{11}C uptake in the liver slowly increased to a maximum at 3 min after injection in all animals (Figure 18B), the radioactivity remained on a plateau and most of the initial uptake was retained after 120 min. In contrast, the ^{18}F liver curves from all animals indicated rapid uptake from arterial blood followed by biexponential clearance and less than 30% of initial liver radioactivity remained after 15 min. In the liver, C-AC is mainly activated by ACS1 in cytosol and is consumed in relatively slow anabolic processes such as lipid and ketone body formation. Far less C-AC reaches the mitochondria and clearance of liver activity is minimal. This is interesting, considering that the liver has a high energy demand and contains approximately 25% of all mitochondria in the body. There was some variability of C-AC retention among the monkeys, probably reflecting a variable metabolic milieu caused by different nutritional status.

7.9.2 Whole-body AC PET-CT studies (Paper Ⅳ)

In monkeys, C-AC accumulated mostly in liver, salivary gland, pancreas, small bowel and spleen (Figure 19A), and was similar to that of pig. But the uptake of salivary gland in pig was less pronounced and higher accumulation was observed in renal cortex, gallbladder wall and bone (Figure 20A). Minimal excretion of C-AC metabolites into bile or urine were observed in either animal. F-AC accumulated mostly in gallbladder, kidney, colon, urinary bladder, and bone in monkeys (Figure 19B). In pig the retention of F-AC was most pronounced in urinary bladder, bone and kidney (Figure 20B). In monkeys 3% of the injected dose ended up in bone and 39% in pig respectively.

A low C-AC uptake in normal brain was observed in this study, similar to the low uptake of cerebellum in Paper Ⅰ and Paper Ⅱ. Acetate does not easily cross the blood-brain barrier and is not extracted from the blood stream as a substrate for neuronal energy metabolism. However, glial cells exhibit acetate uptake by activated ACS2. The carbon label is primarily recovered in the glutamine pool after entering the Krebs cycle [111, 112].

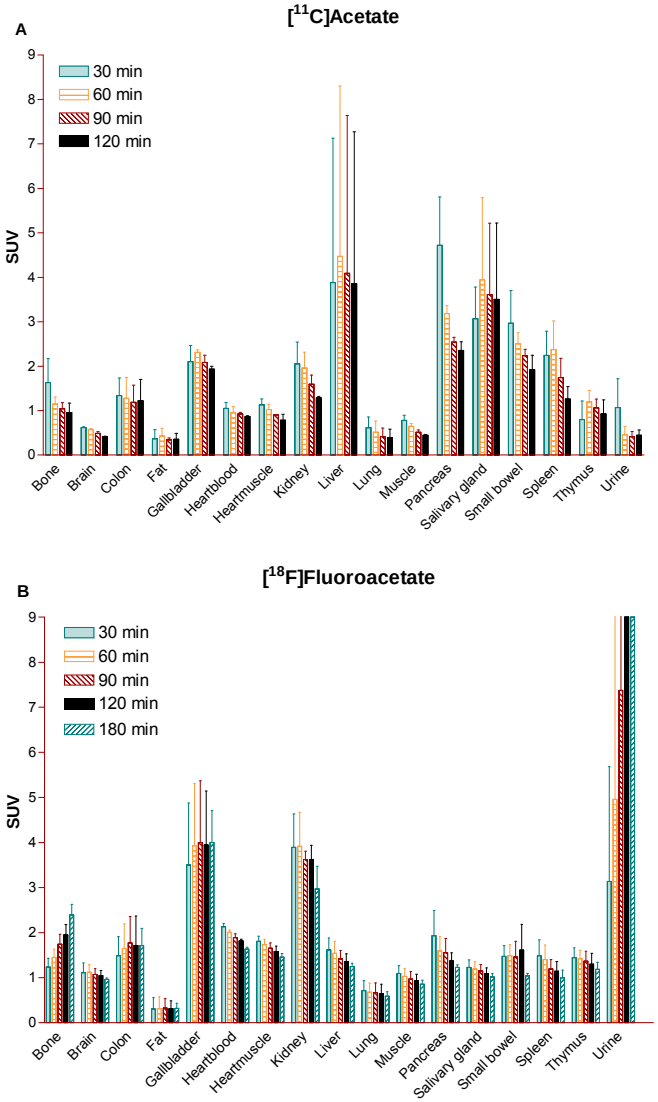

Figure 19 SUVs in different organs at selected time points in cynomolgus monkeys, 1-[^{11}C]Acetate (A) and 2-[^{18}F]Fluoroacetate (B). The bars for urine are truncated, the mean value for 120 and 180 minutes are 12.3 and 21.1 respectively. Derived from Paper Ⅳ.

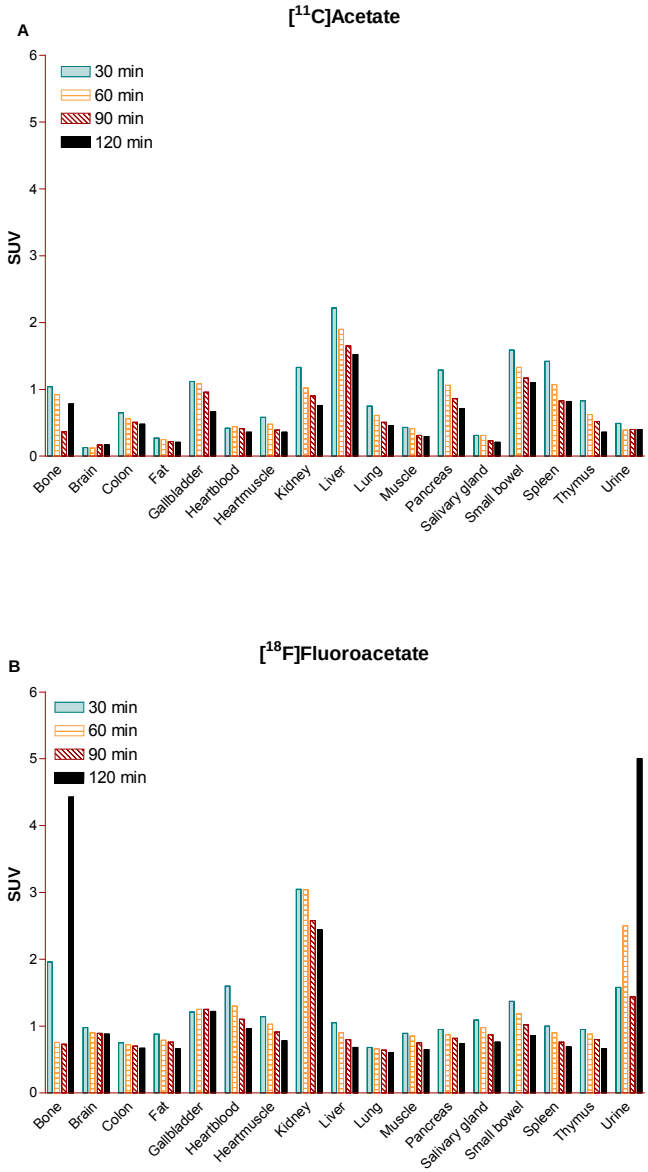

Figure 20 SUVs in different organs at selected time points in domestic pig, (A) 1-[^{11}C]Acetate and (B) 2-[^{18}F]Fluoroacetate. Derived from Paper Ⅳ.

In all animals, radioactivity of F-AC in venous blood was higher than in any mitochondria-rich organs (heart and liver) from 30 min onwards, indicating that intracellular trapping is minimal. In the liver, F-AC was cleared from the blood stream and rapidly excreted to the bile, implying minimal trapping of the fluorinated compound by ACS2 and a poor relation between F-AC retention and lipogenesis. These findings were further supported by lack of prolonged F-AC retention in other lipogenic rich tissues such as salivary gland, pancreas and

spleen. There was minimal loss of carbon-11 activity through urine indicating that massive and expected loss of [^{11}C]-CO_2 were exhaled through the lungs. The main excretion pathways for F-AC were through bile and urine (Figure 21). Defluorination of F-AC was observed in both species, much more obvious in the pig.

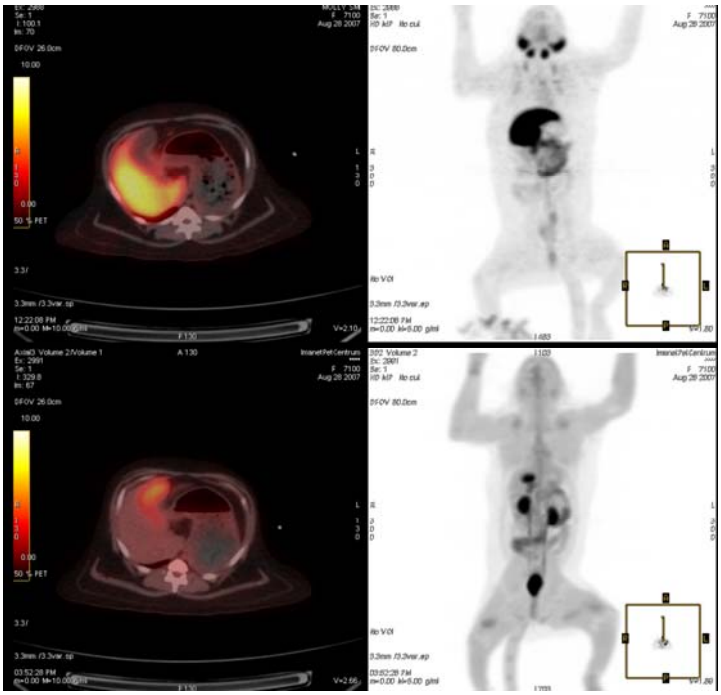

Figure 21 Axial (left) and maximum intensity projection (right) images from whole body scans performed 90 minutes after tracer injection in cynomolgus monkey. Top: 1-[^{11}C]Acetate, bottom: 2-[^{18}F]Fluoroacetate. Derived from Paper Ⅳ.

Although fluoroacetate toxicity is due to formation of fluorocitrate and blocking of the mitochondrial enzyme aconitase, F-AC PET in this study does not seem to trace the intermediary metabolic activity in any organ. This discrepancy is probably related to the fact that symptoms of fluoroacetate poisoning may occur several hours after exposure and at higher doses [86], implying that fluorocitrate formation is a slow process and does not occur within the time window of this study.

No obvious similarities in distribution and retention of the two tracers were seen. F-AC is not an functional analog of C-AC and of little use for evaluating perfusion, intermediary metabolism or lipogenesis.

8 Conclusions

C-AC PET is feasible in detecting primary and lymph node metastases of head and neck squamous cell carcinoma. C-AC PET seems more sensitive than FDG PET for diagnosis and staging the head and neck cancer.

Tumor volumes delineated by C-AC PET resulted in 51% larger than the volumes derived by FDG PET. Both C-AC PET and FDG PET volumes must be carefully validated before used in a clinical setting.

We propose a new non-invasive method for simultaneous assessment of head and neck tumor perfusion and oxidative metabolism in patients using dynamic C-AC PET. This method was used to document a bioenergetic pattern that might predict radioresponsiveness. Restoration of tumor oxidative metabolism might be a potential target for improving the outcome in cancer therapy.

Elevated uptake of C-AC appears to be common in B-LN undergoing fatty degeneration and possibly other processes related to inflammation, but not caused by lymph node drainage from the extremities. High C-AC uptake in a node with tissue density below 15 HU could safely be regarded as benign lymphadenopathy. Combination with density measurement might improve the specificity of C-AC PET in nodal staging of prostate cancer.

Compared to C-AC, F-AC showed prolonged blood retention, undetectable trapping in the myocardium, rapid clearance from liver and excretion to bile and urine. F-AC does not appear to be useful as an functional analog of C-AC for tracing regional perfusion, intermediary metabolism and tissue lipogenesis.

9 Acknowledgements

This work was finished by support from many people in various ways and I would like to express my graceful to

Jens Sörensen, my main supervisor, the clinical director of the Uppsala Imanet PET center, for sharing his vast knowledge and experiences in both research and clinic. For introducing the different research tools needed in my research and for stimulating discussions and well support when I faced difficulties.

Silvia Johansson, my initial main supervisor, now assistant supervisor. For providing me the opportunity to work on this attractive project. For sharing her extensive knowledge about RT and scientific writing and wisdom in both science and life. For understanding my situation as a woman and mother. And for your enthusiasm, encouragement and friendly support.

Prof Mikael Karlsson, my assistant supervisor, for providing me excellent research condition and for understanding and inspiring support, encouragements when I was trapped in dilemmas. Especially for your well organization throughout my study, since I always travel between Uppsala and Umea.

Prof Ingela turesson, my assistant supervisor, for your stimulating discussion and encouragement when my research was trapped in a corner.

Prof Katrine Riklund, my assistant supervisor, for your constructive discussion and encouragement.

Prof Bengt Langstrom, for your stimulating talk and discussion and encouragement.

Örjan Lindhe, Per Nilsson, Lena Cederblad, Jan Bertling, Alexandru Daşu, Cecilia Wassberg for constructive collaboration and excellent linguistic revision and co-authorship.

Lars Lindsjo, for all the energy and patience and you have spent in trying to let me get the proper format data.

Bjorn Jacksson, for your constructive suggestions and friendly help.

Jan Axelsson, physicist of Uppsala Imanet PET center, for sharing your valuable time to help me access the ECAT data.

Lennart thurfjell and Sue Matthews, the managers of GE healthcare, Uppsala Imanet PET center, for providing me an excellent work place and technique support.

Carina, Anna, Pia and Didde, secretaries of oncology department in Umea and Uppsala. For all of your efficiency and plentiful help in lots of practical things. Especially to Carina, you always translate official document into english, this made my life in Sweden much easier.

Qiyu Sun and Jiamin Li, the leader of my hospital in china, for all your support and kindness throughout my study process.

The staff at Uppsala Imanet PET, for all your help and support that you have done for me.

Friends in Sweden and China, for their friendship and giving me recreational times.

My warmest grateful to my parents and my parents in law for their endless love, support and taking care of my daughter during my stay in Sweden. To my sister and brother for their warm-hearted concern and help.

Last, but most to my husband **Xiangkui Mu**, for his never-ending love, support and encouragement during my study, for looking after our child alone when I was not at home, without you, I will never finish this study. And to my lovely daughter **Lele**, for the happiness and fun she had brought to my life and for her looking after herself and doing all well at home and kindergarten without your mother's help.

Thanks the oncology, radiation science department of Umeå university hospital and GE healthcare Uppsala Imanet PET center for giving me warm concern every Christmas.

Thanks the financial supported from Umeå University Lion's Cancer Research Foundation, Uppsala University Amersham PET Research Fund, Laryngfonden and Uppsala University Hospital fund.

Finally I would like to thanks all the patients who participated in this study and made this research possible.

10 References

1. Boyle P, L.B., *World cancer report 2008*. 2008: Lyon International Agency for research on cancer(IARC).
2. Sankaranarayanan, R., et al., *Head and neck cancer: a global perspective on epidemiology and prognosis.* Anticancer Res, 1998. **18**(6B): p. 4779-86.
3. Keyes, J.W., Jr., et al., *FDG PET in head and neck cancer.* AJR Am J Roentgenol, 1997. **169**(6): p. 1663-9.
4. Panje, W.R., et al., *Surgical management of the head and neck cancer patient following concomitant multimodality therapy.* Laryngoscope, 1995. **105**(1): p. 97-101.
5. Lippman, S.M., et al., *Effect of selenium and vitamin E on risk of prostate cancer and other cancers: the Selenium and Vitamin E Cancer Prevention Trial (SELECT).* Jama, 2009. **301**(1): p. 39-51.
6. Parkin, D.M., et al., *Global cancer statistics, 2002.* CA Cancer J Clin, 2005. **55**(2): p. 74-108.
7. Coleman, M.P., et al., *Cancer survival in five continents: a worldwide population-based study (CONCORD).* Lancet Oncol, 2008. **9**(8): p. 730-56.
8. Morris, M.J. and H.I. Scher, *(11)C-acetate PET imaging in prostate cancer.* Eur J Nucl Med Mol Imaging, 2007. **34**(2): p. 181-4.
9. Bernier, J., et al., *Postoperative irradiation with or without concomitant chemotherapy for locally advanced head and neck cancer.* N Engl J Med, 2004. **350**(19): p. 1945-52.
10. Parker, S.L., et al., *Cancer statistics, 1996.* CA Cancer J Clin, 1996. **46**(1): p. 5-27.
11. Vanselow, B., et al., *Oxygenation of advanced head and neck cancer: prognostic marker for the response to primary radiochemotherapy.* Otolaryngol Head Neck Surg, 2000. **122**(6): p. 856-62.
12. Moreno-Sanchez, R., et al., *Energy metabolism in tumor cells.* Febs J, 2007. **274**(6): p. 1393-418.
13. Warburg, O., *On respiratory impairment in cancer cells.* Science, 1956. **124**(3215): p. 269-70.
14. Plathow, C. and W.A. Weber, *Tumor cell metabolism imaging.* J Nucl Med, 2008. **49 Suppl 2**: p. 43S-63S.
15. Gillies, R.J., I. Robey, and R.A. Gatenby, *Causes and consequences of increased glucose metabolism of cancers.* J Nucl Med, 2008. **49 Suppl 2**: p. 24S-42S.
16. Gatenby, R.A. and R.J. Gillies, *A microenvironmental model of carcinogenesis.* Nat Rev Cancer, 2008. **8**(1): p. 56-61.
17. Weber, W.A., *Positron emission tomography as an imaging biomarker.* J Clin Oncol, 2006. **24**(20): p. 3282-92.
18. Fanciulli, M., et al., *Glucose metabolism in adriamycin-sensitive and -resistant LoVo human colon carcinoma cells.* Oncol Res, 1993. **5**(9): p. 357-62.
19. Pelicano, H., et al., *Glycolysis inhibition for anticancer treatment.* Oncogene, 2006. **25**(34): p. 4633-46.

20. Soderberg, K., et al., *The energy charge in wild-type and respiration-deficient Chinese hamster cell mutants.* J Cell Physiol, 1980. **103**(1): p. 169-72.
21. Ristow, M., *Oxidative metabolism in cancer growth.* Curr Opin Clin Nutr Metab Care, 2006. **9**(4): p. 339-45.
22. Jadvar, H., A. Alavi, and S.S. Gambhir, *18F-FDG uptake in lung, breast, and colon cancers: molecular biology correlates and disease characterization.* J Nucl Med, 2009. **50**(11): p. 1820-7.
23. Young, H., et al., *Measurement of clinical and subclinical tumour response using [18F]-fluorodeoxyglucose and positron emission tomography: review and 1999 EORTC recommendations. European Organization for Research and Treatment of Cancer (EORTC) PET Study Group.* Eur J Cancer, 1999. **35**(13): p. 1773-82.
24. Yap, J.T., et al., *Image-guided cancer therapy using PET/CT.* Cancer J, 2004. **10**(4): p. 221-33.
25. Basu, S. and A. Alavi, *Staging with PET and the "Will Rogers" effect: redefining prognosis and survival in patients with cancer.* Eur J Nucl Med Mol Imaging, 2008. **35**(1): p. 1-4.
26. Gregoire, V., et al., *PET-based treatment planning in radiotherapy: a new standard?* J Nucl Med, 2007. **48 Suppl 1**: p. 68S-77S.
27. Salaun, P.Y., et al., *Does (18)fluoro-fluorodeoxyglucose positron emission tomography improve recurrence detection in patients treated for head and neck squamous cell carcinoma with negative clinical follow-up?* Head Neck, 2007. **29**(12): p. 1115-20.
28. Farber, L.A., et al., *Detection of recurrent head and neck squamous cell carcinomas after radiation therapy with 2-18F-fluoro-2-deoxy-D-glucose positron emission tomography.* Laryngoscope, 1999. **109**(6): p. 970-5.
29. Greven, K.M., et al., *Serial positron emission tomography scans following radiation therapy of patients with head and neck cancer.* Head Neck, 2001. **23**(11): p. 942-6.
30. Yao, M., et al., *Pathology and FDG PET correlation of residual lymph nodes in head and neck cancer after radiation treatment.* Am J Clin Oncol, 2007. **30**(3): p. 264-70.
31. McGuirt, W.F., et al., *PET scanning in head and neck oncology: a review.* Head Neck, 1998. **20**(3): p. 208-15.
32. Hannah, A., et al., *Evaluation of 18 F-fluorodeoxyglucose positron emission tomography and computed tomography with histopathologic correlation in the initial staging of head and neck cancer.* Ann Surg, 2002. **236**(2): p. 208-17.
33. Kau, R.J., et al., *Lymph node detection of head and neck squamous cell carcinomas by positron emission tomography with fluorodeoxyglucose F 18 in a routine clinical setting.* Arch Otolaryngol Head Neck Surg, 1999. **125**(12): p. 1322-8.
34. Adams, S., et al., *Prospective comparison of 18F-FDG PET with conventional imaging modalities (CT, MRI, US) in lymph node staging of head and neck cancer.* Eur J Nucl Med, 1998. **25**(9): p. 1255-60.

35. Stokkel, M.P., et al., *Preoperative evaluation of patients with primary head and neck cancer using dual-head 18fluorodeoxyglucose positron emission tomography.* Ann Surg, 2000. **231**(2): p. 229-34.
36. Greven, K.M., *Positron-emission tomography for head and neck cancer.* Semin Radiat Oncol, 2004. **14**(2): p. 121-9.
37. Ford, E.C., et al., *18F-FDG PET/CT for image-guided and intensity-modulated radiotherapy.* J Nucl Med, 2009. **50**(10): p. 1655-65.
38. Nuyts, S., *Defining the target for radiotherapy of head and neck cancer.* Cancer Imaging, 2007. **7 Spec No A**: p. S50-5.
39. Nestle, U., et al., *18F-deoxyglucose positron emission tomography (FDG-PET) for the planning of radiotherapy in lung cancer: high impact in patients with atelectasis.* Int J Radiat Oncol Biol Phys, 1999. **44**(3): p. 593-7.
40. Wang, D., et al., *Initial experience of FDG-PET/CT guided IMRT of head-and-neck carcinoma.* Int J Radiat Oncol Biol Phys, 2006. **65**(1): p. 143-51.
41. Weber, W.A., *Assessing tumor response to therapy.* J Nucl Med, 2009. **50 Suppl 1**: p. 1S-10S.
42. Price, P. and T. Jones, *Can positron emission tomography (PET) be used to detect subclinical response to cancer therapy? The EC PET Oncology Concerted Action and the EORTC PET Study Group.* Eur J Cancer, 1995. **31A**(12): p. 1924-7.
43. Kostakoglu, L. and S.J. Goldsmith, *PET in the assessment of therapy response in patients with carcinoma of the head and neck and of the esophagus.* J Nucl Med, 2004. **45**(1): p. 56-68.
44. Brun, E., et al., *FDG PET studies during treatment: prediction of therapy outcome in head and neck squamous cell carcinoma.* Head Neck, 2002. **24**(2): p. 127-35.
45. Nunez, R., A. Kalapparambath, and J. Varela, *Improvement in sensitivity with delayed imaging of pulmonary lesions with FDG-PET.* Rev Esp Med Nucl, 2007. **26**(4): p. 196-207.
46. Ho, C.L., S.C. Yu, and D.W. Yeung, *11C-acetate PET imaging in hepatocellular carcinoma and other liver masses.* J Nucl Med, 2003. **44**(2): p. 213-21.
47. Oyama, N., et al., *11C-acetate PET imaging of prostate cancer.* J Nucl Med, 2002. **43**(2): p. 181-6.
48. Higashi, K., et al., *11C-acetate PET imaging of lung cancer: comparison with 18F-FDG PET and 99mTc-MIBI SPET.* Eur J Nucl Med Mol Imaging, 2004. **31**(1): p. 13-21.
49. Apolo, A.B., N. Pandit-Taskar, and M.J. Morris, *Novel tracers and their development for the imaging of metastatic prostate cancer.* J Nucl Med, 2008. **49**(12): p. 2031-41.
50. Been, L.B., et al., *[18F]FLT-PET in oncology: current status and opportunities.* Eur J Nucl Med Mol Imaging, 2004. **31**(12): p. 1659-72.
51. Hara, T., et al., *Use of 18F-choline and 11C-choline as contrast agents in positron emission tomography imaging-guided stereotactic biopsy sampling of gliomas.* J Neurosurg, 2003. **99**(3): p. 474-9.

52. Nanni, C., et al., *11C/ 18F-choline PET or 11C/18F-acetate PET in prostate cancer: may a choice be recommended?* Eur J Nucl Med Mol Imaging, 2007. **34**(10): p. 1704-5.
53. Narayanan, T.K., et al., *A comparative study on the uptake and incorporation of radiolabeled methionine, choline and fluorodeoxyglucose in human astrocytoma.* Mol Imaging Biol, 2002. **4**(2): p. 147-56.
54. Yoshimoto, M., et al., *Characterization of acetate metabolism in tumor cells in relation to cell proliferation: acetate metabolism in tumor cells.* Nucl Med Biol, 2001. **28**(2): p. 117-22.
55. Soloviev, D., et al., *PET imaging with 11C-acetate in prostate cancer: a biochemical, radiochemical and clinical perspective.* Eur J Nucl Med Mol Imaging, 2008. **35**(5): p. 942-9.
56. Pike, V.W., et al., *Preparation of [1-11C]acetate--an agent for the study of myocardial metabolism by positron emission tomography.* Int J Appl Radiat Isot, 1982. **33**(7): p. 505-12.
57. Brown, M.A., D.W. Myears, and S.R. Bergmann, *Noninvasive assessment of canine myocardial oxidative metabolism with carbon-11 acetate and positron emission tomography.* J Am Coll Cardiol, 1988. **12**(4): p. 1054-63.
58. Juillard, L., et al., *Validation of renal oxidative metabolism measurement by positron-emission tomography.* Hypertension, 2007. **50**(1): p. 242-7.
59. Wyss, M.T., et al., *Stimulation-induced increases of astrocytic oxidative metabolism in rats and humans investigated with 1-11C-acetate.* J Cereb Blood Flow Metab, 2009. **29**(1): p. 44-56.
60. Ohtsuka, T., et al., *Positive imaging of thymoma by 11C-acetate positron emission tomography.* Ann Thorac Surg, 2006. **81**(3): p. 1132-4.
61. Shibata, H., et al., *11C-acetate for positron emission tomography imaging of clinical stage IA lung adenocarcinoma: comparison with 18F-fluorodeoxyglucose for imaging and evaluation of tumor aggressiveness.* Ann Nucl Med, 2009. **23**(7): p. 609-16.
62. Shreve, P., et al., *Carbon-11-acetate PET imaging in renal disease.* J Nucl Med, 1995. **36**(9): p. 1595-601.
63. Hwang, K.H., et al., *Evaluation of patients with hepatocellular carcinomas using [(11)C]acetate and [(18)F]FDG PET/CT: A preliminary study.* Appl Radiat Isot, 2009. **67**(7-8): p. 1195-8.
64. Liu, R.S., *31. Clinical Application of.* Clin Positron Imaging, 2000. **3**(4): p. 185.
65. Kotzerke, J., et al., *Carbon-11 acetate positron emission tomography can detect local recurrence of prostate cancer.* Eur J Nucl Med Mol Imaging, 2002. **29**(10): p. 1380-4.
66. Oyama, N., et al., *11C-acetate PET imaging of prostate cancer: detection of recurrent disease at PSA relapse.* J Nucl Med, 2003. **44**(4): p. 549-55.
67. Fricke, E., et al., *Positron emission tomography with 11C-acetate and 18F-FDG in prostate cancer patients.* Eur J Nucl Med Mol Imaging, 2003. **30**(4): p. 607-11.
68. Jana, S. and M.D. Blaufox, *Nuclear medicine studies of the prostate, testes, and bladder.* Semin Nucl Med, 2006. **36**(1): p. 51-72.

69. Schoder, H. and S.M. Larson, *Positron emission tomography for prostate, bladder, and renal cancer.* Semin Nucl Med, 2004. **34**(4): p. 274-92.
70. Dimitrakopoulou-Strauss, A. and L.G. Strauss, *PET imaging of prostate cancer with 11C-acetate.* J Nucl Med, 2003. **44**(4): p. 556-8.
71. Vavere, A.L., et al., *1-11C-acetate as a PET radiopharmaceutical for imaging fatty acid synthase expression in prostate cancer.* J Nucl Med, 2008. **49**(2): p. 327-34.
72. Weingartner, K., et al., *Anatomical basis for pelvic lymphadenectomy in prostate cancer: results of an autopsy study and implications for the clinic.* J Urol, 1996. **156**(6): p. 1969-71.
73. McLaughlin, A.P., et al., *Prostatic carcinoma: incidence and location of unsuspected lymphatic metastases.* J Urol, 1976. **115**(1): p. 89-94.
74. Stone, A.R., M.V. Merrick, and G.D. Chisholm, *Prostatic lymphoscintigraphy.* Br J Urol, 1979. **51**(6): p. 556-60.
75. Fowler, J.E., Jr. and W.F. Whitmore, Jr., *The incidence and extent of pelvic lymph node metastases in apparently localized prostatic cancer.* Cancer, 1981. **47**(12): p. 2941-5.
76. Seppala, J., et al., *Carbon-11 acetate PET/CT based dose escalated IMRT in prostate cancer.* Radiother Oncol, 2009. **93**(2): p. 234-40.
77. Mittendorfer, B., et al., *Regional acetate kinetics and oxidation in human volunteers.* Am J Physiol, 1998. **274**(6 Pt 1): p. E978-83.
78. van den Hoff, J., et al., *[1-(11)C]Acetate as a quantitative perfusion tracer in myocardial PET.* J Nucl Med, 2001. **42**(8): p. 1174-82.
79. Luong, A., et al., *Molecular characterization of human acetyl-CoA synthetase, an enzyme regulated by sterol regulatory element-binding proteins.* J Biol Chem, 2000. **275**(34): p. 26458-66.
80. Yoshii, Y., et al., *Tumor uptake of radiolabeled acetate reflects the expression of cytosolic acetyl-CoA synthetase: implications for the mechanism of acetate PET.* Nucl Med Biol, 2009. **36**(7): p. 771-7.
81. Yun, M., et al., *The importance of acetyl coenzyme A synthetase for 11C-acetate uptake and cell survival in hepatocellular carcinoma.* J Nucl Med, 2009. **50**(8): p. 1222-8.
82. Yeh, S.H., et al., *11C-acetate clearance in nasopharyngeal carcinoma.* Nucl Med Commun, 1999. **20**(2): p. 131-4.
83. Klein, L.J., et al., *Carbon-11 acetate as a tracer of myocardial oxygen consumption.* Eur J Nucl Med, 2001. **28**(5): p. 651-68.
84. Ishiwata, K., et al., *Evaluation of O-[11C]methyl-L-tyrosine and O-[18F]fluoromethyl-L-tyrosine as tumor imaging tracers by PET.* Nucl Med Biol, 2004. **31**(2): p. 191-8.
85. Krohn, K.A., D.A. Mankoff, and J.F. Eary, *Imaging cellular proliferation as a measure of response to therapy.* J Clin Pharmacol, 2001. **Suppl**: p. 96S-103S.
86. Goncharov, N.V., R.O. Jenkins, and A.S. Radilov, *Toxicology of fluoroacetate: a review, with possible directions for therapy research.* J Appl Toxicol, 2006. **26**(2): p. 148-61.
87. Ponde, D.E., et al., *18F-fluoroacetate: a potential acetate analog for prostate tumor imaging--in vivo evaluation of 18F-fluoroacetate versus 11C-acetate.* J Nucl Med, 2007. **48**(3): p. 420-8.

88. Marik, J., et al., *PET of glial metabolism using 2-18F-fluoroacetate.* J Nucl Med, 2009. **50**(6): p. 982-90.
89. Therasse, P., *Evaluation of response: new and standard criteria.* Ann Oncol, 2002. **13 Suppl 4**: p. 127-9.
90. Delbeke, D., et al., *Procedure guideline for tumor imaging with 18F-FDG PET/CT 1.0.* J Nucl Med, 2006. **47**(5): p. 885-95.
91. Kaji, M., et al., *11C-acetate and 18F-fluorodeoxyglucose positron emission tomography of pulmonary adenocarcinoma.* Ann Thorac Surg, 2007. **83**(1): p. 312-4.
92. Grosu, A.L., et al., *Positron emission tomography for radiation treatment planning.* Strahlenther Onkol, 2005. **181**(8): p. 483-99.
93. Nestle, U., et al., *Comparison of different methods for delineation of 18F-FDG PET-positive tissue for target volume definition in radiotherapy of patients with non-Small cell lung cancer.* J Nucl Med, 2005. **46**(8): p. 1342-8.
94. Schwartz, D.L., et al., *FDG-PET/CT-guided intensity modulated head and neck radiotherapy: a pilot investigation.* Head Neck, 2005. **27**(6): p. 478-87.
95. Black, Q.C., et al., *Defining a radiotherapy target with positron emission tomography.* Int J Radiat Oncol Biol Phys, 2004. **60**(4): p. 1272-82.
96. Paulino, A.C. and P.A. Johnstone, *FDG-PET in radiotherapy treatment planning: Pandora's box?* Int J Radiat Oncol Biol Phys, 2004. **59**(1): p. 4-5.
97. Yu, H., et al., *Automated radiation targeting in head-and-neck cancer using region-based texture analysis of PET and CT images.* Int J Radiat Oncol Biol Phys, 2009. **75**(2): p. 618-25.
98. Armbrecht, J.J., D.B. Buxton, and H.R. Schelbert, *Validation of [1-11C]acetate as a tracer for noninvasive assessment of oxidative metabolism with positron emission tomography in normal, ischemic, postischemic, and hyperemic canine myocardium.* Circulation, 1990. **81**(5): p. 1594-605.
99. Zhou, S., et al., *Frequency and phenotypic implications of mitochondrial DNA mutations in human squamous cell cancers of the head and neck.* Proc Natl Acad Sci U S A, 2007. **104**(18): p. 7540-5.
100. Papandreou, I., et al., *HIF-1 mediates adaptation to hypoxia by actively downregulating mitochondrial oxygen consumption.* Cell Metab, 2006. **3**(3): p. 187-97.
101. Lopez-Rios, F., et al., *Loss of the mitochondrial bioenergetic capacity underlies the glucose avidity of carcinomas.* Cancer Res, 2007. **67**(19): p. 9013-7.
102. Silva, S.D., et al., *Expression of fatty acid synthase, ErbB2 and Ki-67 in head and neck squamous cell carcinoma. A clinicopathological study.* Oral Oncol, 2004. **40**(7): p. 688-96.
103. van Waveren, C., et al., *Oxidative phosphorylation dysfunction modulates expression of extracellular matrix--remodeling genes and invasion.* Carcinogenesis, 2006. **27**(3): p. 409-18.
104. Laking, G.R., et al., *Imaging vascular physiology to monitor cancer treatment.* Crit Rev Oncol Hematol, 2006. **58**(2): p. 95-113.

105. Ponto, L.L., et al., *Assessment of Blood Flow in Solid Tumors Using PET.* Clin Positron Imaging, 1998. **1**(2): p. 117-121.
106. Oyama, N., et al., *MicroPET assessment of androgenic control of glucose and acetate uptake in the rat prostate and a prostate cancer tumor model.* Nucl Med Biol, 2002. **29**(8): p. 783-90.
107. Malmstrom, P.U., *Lymph node staging in prostatic carcinoma revisited.* Acta Oncol, 2005. **44**(6): p. 593-8.
108. Golimbu, M., et al., *Extended pelvic lymphadenectomy for prostatic cancer.* J Urol, 1979. **121**(5): p. 617-20.
109. Heidenreich, A., Z. Varga, and R. Von Knobloch, *Extended pelvic lymphadenectomy in patients undergoing radical prostatectomy: high incidence of lymph node metastasis.* J Urol, 2002. **167**(4): p. 1681-6.
110. Leborgne, R., F. Leborgne, Jr., and J.H. Leborgne, *Soft-Tissue Radiography of Axillary Nodes with Fatty Infiltration.* Radiology, 1965. **84**: p. 513-5.
111. Dienel, G.A., et al., *Preferential labeling of glial and meningial brain tumors with [2-(14)C]acetate.* J Nucl Med, 2001. **42**(8): p. 1243-50.
112. Hosoi, R., et al., *Sensitive reduction in 14C-acetate uptake in a short-term ischemic rat brain.* J Stroke Cerebrovasc Dis, 2007. **16**(2): p. 77-81.